HHS Public Access

Author manuscript

Sci Signal. Author manuscript; available in PMC 2017 February 08.

Published in final edited form as:

Sci Signal. ; 10(463): . doi:10.1126/scisignal.aaf9647.

Ser[1928] phosphorylation by PKA stimulates the L-type Ca^{2+} channel $Ca_V1.2$ and vasoconstriction during acute hyperglycemia and diabetes

Matthew A. Nystoriak[1,*], **Madeline Nieves-Cintrón**[1], **Tommaso Patriarchi**[1], **Olivia R. Buonarati**[1], **Maria Paz Prada**[1], **Stefano Morotti**[1], **Eleonora Grandi**[1], **Julia Dos Santos Fernandes**[1], **Katherine Forbush**[2], **Franz Hofmann**[3], **Kent C. Sasse**[4], **John D. Scott**[2], **Sean M. Ward**[5], **Johannes W. Hell**[1], and **Manuel F. Navedo**[1,†]

[1]Department of Pharmacology, University of California, Davis, Davis, CA 95616, USA.

[2]Howard Hughes Medical Institute and Department of Pharmacology, University of Washington, Seattle, WA 98195, USA.

[3]Department of Pharmacology and Toxicology, Technical University of Munich, Munich D80802, Germany.

[4]Sasse Surgical Associates, Reno, NV 89502, USA.

[5]Department of Physiology and Cell Biology, University of Nevada, Reno, NV 89557, USA.

Abstract

Hypercontractility of arterial myocytes and enhanced vascular tone during diabetes are, in part, attributed to the effects of increased glucose (hyperglycemia) on L-type $Ca_V1.2$ channels. In murine arterial myocytes, kinase-dependent mechanisms mediate the increase in $Ca_V1.2$ activity in response to increased extracellular glucose. We identified a subpopulation of the $Ca_V1.2$ channel pore-forming subunit ($\alpha 1_C$) within nanometer proximity of protein kinase A (PKA) at the sarcolemma of murine and human arterial myocytes. This arrangement depended upon scaffolding of PKA by an A-kinase anchoring protein 150 (AKAP150) in mice. Glucose-mediated increases in $Ca_V1.2$ channel activity were associated with PKA activity, leading to $\alpha 1_C$ phosphorylation at Ser[1928]. Compared to arteries from low-fat diet (LFD)–fed mice and nondiabetic patients, arteries

†Corresponding author. mfnavedo@ucdavis.edu.

*Present address: Diabetes and Obesity Center, Department of Medicine, University of Louisville, 580 South Preston Street, Delia Baxter, Louisville, KY 40202, USA.

SUPPLEMENTARY MATERIALS

www.sciencesignaling.org/cgi/content/full/10/463/eaaf9647/DC1

Author contributions: M.A.N. and M.F.N. conceived, designed, and executed experiments; collected, analyzed, and interpreted data; and wrote and revised the manuscript. M.N.-C., T.P., O.R.B., M.P.P., S.M., E.G., and J.D.S.F. executed experiments; collected, interpreted, and analyzed data; and revised the manuscript. K.C.S. and S.M.W. contributed human samples critical to this work and basic information about patients and revised the manuscript. K.F., F.H., and J.D.S. contributed genetically modified mice critical to this work and revised the manuscript. J.W.H. interpreted results, contributed specimens critical to this work, and revised the manuscript.

Competing interests: K.C.S. is on the Scientific Advisory Board of ACell Corporation. All other authors declare that they have no competing interests.

Data and materials availability: Genetically modified mice require a material transfer agreement from the University of Munich (S1928A knockin mice) and University of Washington, Seattle, WA (*AKAP150*$^{-/-}$, ΔA, and ΔC mice).

from high-fat diet (HFD)–fed mice and from diabetic patients had increased Ser^{1928} phosphorylation and $Ca_V1.2$ activity. Arterial myocytes and arteries from mice lacking AKAP150 or expressing mutant AKAP150 unable to bind PKA did not exhibit increased Ser^{1928} phosphorylation and $Ca_V1.2$ current density in response to increased glucose or to HFD. Consistent with a functional role for Ser^{1928} phosphorylation, arterial myocytes and arteries from knockin mice expressing a $Ca_V1.2$ with Ser^{1928} mutated to alanine (S1928A) lacked glucose-mediated increases in $Ca_V1.2$ activity and vasoconstriction. Furthermore, the HFD-induced increases in $Ca_V1.2$ current density and myogenic tone were prevented in S1928A knockin mice. These findings reveal an essential role for $\alpha 1_C$ phosphorylation at Ser^{1928} in stimulating $Ca_V1.2$ channel activity and vasoconstriction by AKAP-targeted PKA upon exposure to increased glucose and in diabetes.

INTRODUCTION

Diabetes mellitus is a major risk factor underlying multiple pathological complications such as stroke, hypertension, heart disease, and retinal degeneration (1). These pathologies have been linked, in part, to enhanced contractility of arterial myocytes in the resistance vasculature during hyperglycemia, that is, high blood glucose that is a signature metabolic feature of diabetes (2–7). The contractile state of arterial myocytes, and thereby arterial diameter, is predominantly controlled by the amount of Ca^{2+} influx through L-type $Ca_V1.2$ channels. We reported that $Ca_V1.2$ channel activity in murine cerebral arterial myocytes is augmented in response to increased glucose and in a mouse model of diabetes through a process that is independent of changes in membrane potential (8). However, the molecular mechanisms underlying the enhanced $Ca_V1.2$ channel function associated with increased glucose and whether similar phenomena are engaged in the human vasculature during diabetes are unclear.

The physiological importance of $Ca_V1.2$ channels is underscored by their essential role in cardiac contractility, neuronal excitability, and control of vascular tone in health and disease (9, 10). $Ca_V1.2$ channels are composed of pore-forming $\alpha 1_C$ subunits in association with several regulatory accessory subunits (11). Regulation of $Ca_V1.2$ function occurs through reversible phosphorylation of the channel complex by serine/threonine kinases and phosphatases, including protein kinase A (PKA) (10–12). Modulation of $Ca_V1.2$ channel function by PKA has been extensively studied in the context of β-adrenergic stimulation in the heart and brain (9, 12). Although PKA-dependent stimulation of $Ca_V1.2$ channels occurs in myocytes from arteries and portal veins (13–15), the molecular mechanisms and functional implications are unknown.

Regulation of $Ca_V1.2$ channel activity by PKA in other cell types involves direct phosphorylation of one or more subunits that compose the channel (16). A highly conserved PKA consensus phosphorylation site is Ser^{1928}, located within the intracellular C terminus of $\alpha 1_C$. Stimulation of $Ca_V1.2$ by PKA activity has been associated with increased phosphorylation of this residue in neurons (17–20) and cardiac cells (19), although its physiological significance in cardiac $Ca_V1.2$ channel function is controversial (21, 22).

However, evidence for this modification and elucidation of its functional role in the vasculature are lacking.

PKA-dependent stimulation of heterologously expressed (23), as well as native cardiac (24, 25) and neuronal (20, 26, 27), $Ca_V1.2$ channels requires an A-kinase anchoring protein (AKAP) scaffold. Consistent with these findings, we demonstrated that potentiation of $Ca_V1.2$ channels in arterial myocytes during acute increases in extracellular D-glucose requires an AKAP-bound PKA (8). Yet, the functional implications of PKA-dependent stimulation of $Ca_V1.2$ channels in response to increased glucose, as well as the identity of the AKAP, are unknown. Here, super-resolution nanoscopy and analysis by proximity ligation assay (PLA) revealed the existence of a subpopulation of $Ca_V1.2$ and PKA catalytic subunit (PKA_{cat}) clusters that are within nanometer range of each other in mouse and human arterial myocytes. We identified the scaffold protein AKAP150 (the murine ortholog of human AKAP79) and the binding of PKA to AKAP150 as key determinants of PKA-mediated $\alpha 1_C$ phosphorylation at Ser^{1928}. PKA-mediated phosphorylation of this residue resulted in potentiation of vascular $Ca_V1.2$ channel activity and vasoconstriction in response to increased extracellular D-glucose. Enhanced $Ca_V1.2$ channel activity and intracellular Ca^{2+} concentrations ($[Ca^{2+}]_i$), which augmented vasoconstriction in response to increased D-glucose and in mice fed a high-fat diet (HFD), were abolished upon prevention of Ser^{1928} phosphorylation by selective mutation of this residue to alanine in S1928A knockin mice. We also observed PKA-dependent phosphorylation of $\alpha 1_C$ at Ser^{1928} and enhanced $Ca_V1.2$ channel activity in human arterial myocytes in response to increased extracellular D-glucose and in human cells from diabetic subjects, thus highlighting the translational relevance of our findings. Together, these results revealed a fundamental role for AKAP-dependent, PKA-meditated phosphorylation of $\alpha 1_C$ at Ser^{1928} as a key molecular signaling event underlying potentiation of $Ca_V1.2$ channel activity and vasoconstriction upon acute increases in extracellular D-glucose and in diabetes.

RESULTS

Super-resolution spatial maps and PLA reveal sarcolemmal $Ca_V1.2$-PKA interactions

Enhanced $Ca_V1.2$ channel activity in rodent cerebral arterial myocytes after an increase in extracellular D-glucose depends upon PKA activity (8). We therefore hypothesized that a subpopulation of PKA is located near $Ca_V1.2$ channels in these cells, enabling functional regulation of channel activity. To test this, we examined the spatial relationship between $Ca_V1.2$ and PKA in freshly dissociated cerebral arterial myocytes from wild-type mice using stochastic optical reconstruction microscopy (STORM) in the total internal reflection fluorescence (TIRF) configuration with antibodies against $Ca_V1.2$ (28) and PKA_{cat}. This method achieves a lateral resolution of ~30 nm with selective axial illumination of sarcolemmal and subsarcolemmal regions. Although conventional TIRF images showed diffuse and regionally varied fluorescence associated with $Ca_V1.2$ and PKA_{cat} (Fig. 1A, top), STORM-rendered spatial maps revealed that both proteins were broadly distributed in clusters of various sizes ($Ca_V1.2$, 2485 ± 47 nm^2; PKA_{cat}, 3272 ± 72 nm^2) at the sarcolemma of arterial myocytes [Fig. 1, A (bottom) and B]. We observed sites of close interaction between $Ca_V1.2$ and PKA_{cat} (Fig. 1C). Histograms of the $Ca_V1.2$-to-nearest

PKA_{cat} distances were fit with a two-component Gaussian function with centers at ~93 and ~256 nm (Fig. 1D), suggesting that a pool of PKA is localized closer to a subpopulation (~5 to 10%) of $Ca_V1.2$ channels.

We used PLA as an additional test of $Ca_V1.2$-PKA association in arterial myocytes. PLA generates fluorescent puncta when proteins of interest are at or less than 40 nm apart (29). Mouse arterial myocytes colabeled for $Ca_V1.2$ and PKA_{cat} produced fluorescent puncta, indicating the presence of the PLA reaction product (Fig. 1E). PLA signals were nearly absent when either $Ca_V1.2$ or PKA_{cat} primary antibodies were omitted (Fig. 1, E and F). PLA was also performed on cells colabeled for $Ca_V1.2$ and transferrin receptor (TfR) or $Ca_V1.2$ and the Ca^{2+}-activated Cl^- channel anoctamin 1 (ANO1), which are cell surface proteins that have limited to no interaction with $Ca_V1.2$ (30–33). Arterial myocytes were robustly stained for TfR and ANO1 when primary antibodies were included in the preparation (fig. S1A), yet no PLA signal was detected in cells colabeled for $Ca_V1.2$ and TfR or $Ca_V1.2$ and ANO1 (fig. S1, B and C). As a positive control, cells colabeled with two distinct $Ca_V1.2$ antibodies [rabbit FP1 (28) and monoclonal NeuroMab clone N263/31] showed surface membrane staining (fig. S1A) and produced robust PLA signals (fig. S1, B and C). Together, these data indicated close (≲40 nm) spatial proximity between a subpopulation of $Ca_V1.2$ channels and PKA_{cat} in mouse arterial myocytes.

AKAP150 facilitates sarcolemmal interactions between $Ca_V1.2$ and PKA in murine arterial myocytes

The scaffolding protein AKAP150, which is the murine ortholog of human AKAP79, binds and coordinates a multienzyme complex that includes PKA, protein kinase C (PKC), and the protein phosphatase calcineurin to facilitate signaling to specific substrates, including $Ca_V1.2$ (20, 26, 27, 34–37). We found that the PKA RIIα regulatory subunit and PKCα coimmuno-precipitated with AKAP150 in arteries from wild-type mice (Fig. 2A). We tested whether the AKAP150-PKA complex facilitates the proximity between PKA_{cat} and $Ca_V1.2$ in arterial myocytes by examining their distribution in cells isolated from two genetically engineered mouse strains. One expresses a truncated form of AKAP150 in which the binding site for PKA has been deleted (ΔA; fig. S2) (26, 38), and the other lacks the entire AKAP150 protein (*AKAP150*$^{-/-}$) (37). The association between AKAP150 and PKA RIIα was either absent (*AKAP150*$^{-/-}$) or markedly reduced (ΔA) in arteries from these mice (Fig. 2A). Coimmunoprecipitation of PKCα within the AKAP150 complex was maintained in ΔA arteries but was absent in the arteries from the *AKAP150*$^{-/-}$ mice (Fig. 2A).

We used structured illumination microscopy (SIM; lateral resolution, ~114 nm) (39) in combination with an object-based analysis to compare $Ca_V1.2$ and PKA_{cat} proximity in arterial myocytes from wild-type, ΔA, and *AKAP150*$^{-/-}$ animals. Consistent with findings we obtained by STORM, object-based analysis identified sites of spatial overlap between $Ca_V1.2$ and PKA_{cat} at the sarcolemma of wild-type arterial myocytes (Fig. 2, B to D). In contrast, cells from ΔA and *AKAP150*$^{-/-}$ mice exhibited significantly fewer sites of overlap between $Ca_V1.2$ and PKA_{cat} (Fig. 2, B and D). Furthermore, ΔA and *AKAP150*$^{-/-}$ myocytes had a reduction in the density of PKA_{cat} but not $Ca_V1.2$ particles at the sarcolemma

identified by STORM/TIRF (Fig. 2E). These findings suggested that AKAP150 facilitates targeting of a pool of PKA_{cat} to a subpopulation of $Ca_V1.2$ in arterial myocytes.

Enhanced vascular $Ca_V1.2$ current in 20 mM D-glucose requires AKAP150-anchored PKA

We tested the hypothesis that increasing extracellular D-glucose from 10 to 20 mM augments $Ca_V1.2$ channel activity in an AKAP150- and PKA-dependent manner in mouse arterial myocytes. These extracellular D-glucose concentrations are within the range of observed nonfasting blood glucose concentrations reported for nondiabetic and experimental diabetic mice, respectively (3, 8, 40). To assess the effects of increased extracellular glucose on $Ca_V1.2$ channel activity, we used patch-clamp electrophysiology in the whole-cell configuration with barium (Ba^{2+}) as the charge carrier before and after application of the L-type calcium channel blocker nifedipine to determine the nifedipine-sensitive Ba^{2+} current (I_{Ba}) associated with $Ca_V1.2$ channel activity. We found that 20 mM D-glucose produced a robust increase in I_{Ba} across a range of membrane potentials with no change in the current-voltage (*I-V*) relationship (V_{max} = 8.75 ± 1.26 mV for 10 mM D-glucose and V_{max} = 9.45 ± 0.56 mV for 20 mM D-glucose; P = 0.6174, extra sum-of-squares F test) in arterial myocytes (Fig. 3, A and B). We also observed a similar increase in I_{Ba} in response to 20 mM D-glucose in mesenteric and femoral arterial myocytes (fig. S3, A and B), suggesting that increased extracellular D-glucose potentiates $Ca_V1.2$ current density in myocytes from different vascular beds. Incubation of arterial myocytes with the selective inhibitor of the glucose transporter GLUT4 indinavir (41) prevented the increase in $Ca_V1.2$ current density in response to 20 mM D-glucose (fig. S4A). Furthermore, I_{Ba} was unchanged when D-glucose was substituted with equimolar concentrations of the metabolically inactive enantiomer L-glucose (10 mM D-glucose + 10 mM L-glucose; fig. S4B), suggesting that enhanced $Ca_V1.2$ channel activity in response to increased D-glucose requires its internalization and metabolic utilization.

Contrary to findings in wild-type arterial myocytes, 20 mM G-glucose did not stimulate I_{Ba} that were elicited with a voltage pulse from −70 to +10 mV in *AKAP150*$^{-/-}$ and ΔA myocytes (Fig. 3, C and D). Note that there was no change in *I-V* relationship by 20 mM D-glucose in *AKAP150*$^{-/-}$ cells (fig. S5) with V_{max} similar to that in wild-type cells (V_{max} = 8.75 ± 1.26 mV in wild-type and V_{max} = 7.98 ± 2.06 mV in *AKAP150*$^{-/-}$; P = 0.7836, extra sum-of-squares F test). Consistent with the electrophysiological data, we observed an increase in $[Ca^{2+}]_i$ in cells from wild-type mice loaded with the Ca^{2+}-sensitive indicator Fluo-4 in response to 20 mM D-glucose (Fig. 3, E and F). This response was not observed in the presence of nifedipine or when D-glucose was substituted with L-glucose (fig. S6), and it was significantly attenuated in *AKAP150*$^{-/-}$ and ΔA cells (Fig. 3, E and F). Together, these findings indicated that AKAP150-anchored PKA signaling is required for enhanced $Ca_V1.2$ channel activity and an increase in global $[Ca^{2+}]_i$ in response to increasing the concentration of extracellular D-glucose.

We also investigated whether AKAP150-anchored PKC participates in enhancing I_{Ba} in response to increasing extracellular D-glucose to 20 mM with a transgenic mouse expressing a form of AKAP150 that cannot bind PKC, yet retains binding to PKA (ΔC; Fig. 4A and fig. S2). Consistent with results in arteries from *AKAP150*$^{-/-}$ mice (37), basal tone in

pressurized (60 mmHg) middle cerebral arteries was slightly reduced in the ΔC mice, and receptor-mediated activation of PKC with angiotensin II evoked less constriction in arteries from ΔC mice than in arteries from littermate controls (Fig. 4, B to D). Moreover, angiotensin II did not increase I_{Ba} in arterial myocytes from ΔC mice, yet I_{Ba} in these cells was significantly augmented by 20 mM D-glucose (Fig. 4, E and F). These data indicated that AKAP150-anchored PKA, but not AKAP150-anchored PKC, is responsible for enhanced $Ca_V1.2$ channel activity in response to increased D-glucose in arterial myocytes.

Phosphorylation of $\alpha1_C$ at Ser^{1928} underlies enhanced vascular $Ca_V1.2$ activity in response to 20 mM D-glucose

We tested whether increased $Ca_V1.2$ channel activity was associated with an alteration in the phosphorylation state of the $\alpha1_C$ subunit at Ser^{1928}, which is a conserved PKA target site in the distal C terminus and which has been implicated in $Ca_V1.2$ regulation (17–19). Using Western blot analysis with a specific antibody that recognizes $\alpha1_C$ phosphorylation at Ser^{1928} (42), we found increased phosphorylation of this residue in wild-type mouse arterial lysates incubated for 5 min with 20 mM D-glucose as compared with those with 10 mM D-glucose (Fig. 5, A and B). In contrast to wild-type arteries, no change in Ser^{1928} phosphorylation in response to 20 mM D-glucose was observed in arterial lysates from ΔA or *AKAP150*$^{-/-}$ mice (Fig. 5, A and B). These results suggested that AKAP150-anchored PKA is required for phosphorylation of $\alpha1_C$ at Ser^{1928} in response to increased D-glucose.

Considering an apparent relationship in molecular and functional data described above, we postulated that Ser^{1928} serves as a functional PKA regulatory site in vascular $Ca_V1.2$ channels. This hypothesis was tested using patch-clamp electrophysiology to record I_{Ba} in arterial myocytes isolated from a genetically engineered mouse expressing $Ca_V1.2$ in which Ser^{1928} has been mutated to an alanine residue (S1928A) (21). Our data revealed that I_{Ba} was not altered by an increase in extracellular D-glucose in S1928A myocytes (Fig. 5, C and D). Pretreatment of wild-type myocytes with the PKA inhibitor Rp-cyclic 3′,5′-hydrogen phosphorothioate adenosine triethylammonium salt (rpcAMPS) also blocked the D-glucose–induced stimulation of I_{Ba} (Fig. 5, C and D). In contrast to the response of wild-type cells, we found no significant change in global $[Ca^{2+}]_i$ in response to 20 mM D-glucose in cells from S1928A mice (Fig. 5E). We confirmed that protein abundance of $K_V2.1$, BK_{Ca} α, and BK_{Ca} β1 subunits, which regulate arterial myocyte excitability and are glucose-sensitive (43–46), is similar between wild-type and S1928A arteries (fig. S7), thus suggesting that loss of glucose-induced stimulation of global Ca^{2+} in S1928A myocytes is not due to changes in basal expression of these K^+ channel subunits.

Increases in extracellular D-glucose could modulate protein function by promoting O-linked *N*-acetylglucosamine (O-GlcNAc) (47, 48). Therefore, we examined whether posttranslational O-GlcNAc modification modulates $Ca_V1.2$ channel activity in response to increased D-glucose by treating wild-type cells with the inhibitor of glutaminefructose amidotransferase, 6-diazo-5-oxo-L-norleucine (DON), and measuring the effect of glucose on I_{Ba}. Inhibition of this enzyme prevents production of the substrate for O-GlcNAc transferase. Perfusion of 20 mM D-glucose enhanced I_{Ba} in wild-type mouse arterial

myocytes in the presence of DON, indicating that the effect of glucose on $Ca_V1.2$ channel activity was not mediated by O-GlcNAcylation (fig. S8).

To explore the functional significance of the glucose-induced Ser^{1928} phosphorylation, we performed measurements of arterial diameter in pressurized (60 mmHg) middle cerebral arteries in the presence of 10 and 20 mM D-glucose. Arteries isolated from wild-type mice developed stable myogenic tone and constricted in response to 20 mM D-glucose (Fig. 5F). This constriction response was independent of endothelial function, because we observed a similar response in wild-type endotheliumdenuded arteries (fig. S9). Although basal myogenic tone was not significantly different in arteries from S1928A and wild-type mice, the response to 20 mM D-glucose was abolished in arteries from S1928A mice (Fig. 5F). Together, data indicated that phosphorylation of $\alpha 1_C$ at Ser^{1928} by AKAP150-anchored PKA is necessary for increased $Ca_V1.2$ channel activity, global $[Ca^{2+}]_i$, and vasoconstriction in response to 20 mM D-glucose.

The single point mutation S1928A restores normal $Ca_V1.2$ activity and vascular tone in HFD animals

We tested whether phosphorylation of $\alpha 1_C$ at Ser^{1928} is enhanced in mice on an HFD. Wild-type, *AKAP150*$^{-/-}$, ΔA, and S1928A animals were maintained on either a low-fat diet (LFD) (10% kcal fat) or HFD (60% kcal fat) for a period of 12 to 16 weeks. This HFD model recapitulates clinical features observed in patients with type 2 diabetes (49, 50), including enhanced arterial tone and increased blood pressure (3, 40). HFD animals exhibited significantly higher body weight and increased blood glucose concentration (table S1). Arteries and arterial myocytes from LFD and HFD mice were isolated, maintained, and immediately used in experiments with extracellular solutions containing 10 mM D-glucose. We found that $\alpha 1_C$ at Ser^{1928} was significantly more phosphorylated in arteries from wild-type HFD mice compared with those from wild-type LFD mice (Fig. 6, A and B). Additionally, arteries from the LFD and HFD ΔA mice had similar amounts of Ser^{1928} phosphorylation, which were not different compared with arteries from wild-type LFD mice (Fig. 6, A and B). Arterial myocytes from wild-type HFD mice exhibited significant enhancement of I_{Ba} over a range of membrane potentials with no change in *I-V* relationship (V_{max} = 7.66 ± 0.87 mV for LFD and V_{max} = 6.94 ± 1.21 mV for HFD; P = 0.7075, extra sum-of-squares F test) (Fig. 6C and fig. S10). Yet, enhanced I_{Ba} was absent in arterial myocytes from *AKAP150*$^{-/-}$, ΔA, or S1928A HFD mice (Fig. 6C and fig. S10).

We also examined the relevance of Ser^{1928} phosphorylation on the development of myogenic tone in diabetic mice. Vasoconstriction in response to 60 mM K^+, in which membrane potential closely follows the equilibrium potential for K^+ (~−20 mV) (51), was significantly higher in arteries from wild-type HFD mice, but not in arteries from S1928A HFD mice, compared with those from corresponding LFD mice (table S2). In line with other reports (3, 40), arteries from wild-type HFD mice consistently developed greater myogenic tone compared to arteries from wild-type LFD mice over a range of intravascular pressures (Fig. 6, D and E). Arterial tone development was not different between arteries from HFD or LFD wild-type mice in the presence of the L-type calcium channel blocker nifedipine (fig. S11), suggesting that the greater myogenic response in HFD mice requires $Ca_V1.2$ activity. In

contrast to the findings in arteries from wild-type mice, arterial tone was similar between arteries from S1928A mice on LFD and HFD at all intravascular pressures tested (Fig. 6, D and E). Together, these findings indicated a key role for AKAP150-anchored PKA, leading to phosphorylation of $\alpha 1_C$ at Ser^{1928} in stimulation of $Ca_V1.2$ channel activity in HFD mice. Our results suggested that substitution of a single amino acid (Ser to Ala at residue 1928) to block Ser^{1928} phosphorylation in the $\alpha 1_C$ is sufficient to prevent the increase in $Ca_V1.2$ channel activity and vascular tone in HFD mice.

PKA mediates phosphorylation of $\alpha 1_C$ at Ser^{1928} and increased $Ca_V1.2$ activity in native human arterial myocytes from diabetic subjects

To test the translational significance of our observations, we analyzed native human arterial myocytes and arteries from nondiabetic and diabetic patients (table S3). In native contractile human arterial myocytes from nondiabetic patients, STORM/TIRF and PLA imaging revealed a subpopulation of $Ca_V1.2$ within close proximity to PKA_{cat} (Fig. 7, A and B, and fig. S12), similar to our results in murine arterial myocytes (Fig. 1). We tested a role for PKA in Ser^{1928} phosphorylation and $Ca_V1.2$ channel activity in response to increasing extracellular D-glucose from 5 to 15 mM in native human arterial myocytes from nondiabetic patients. We selected these concentrations because they are comparable to the blood glucose concentrations observed in nondiabetic and diabetic subjects. We found that 15 mM D-glucose increased I_{Ba} in cells from nondiabetic human subjects (Fig. 7, C and D). Global $[Ca^{2+}]_i$ also significantly increased in response to 15 mM D-glucose in these cells, and this effect was attenuated by inhibition of PKA with rpcAMPS (Fig. 7, E and F). Moreover, incubation with 15 mM D-glucose for 5 min stimulated a significant increase in phosphorylation of $\alpha 1_C$ at Ser^{1928} in intact arteries from the non-diabetic subjects (Fig. 7, G and H). Preincubating the arteries in rpcAMPS abolished this increase, indicating that Ser^{1928} phosphorylation during increased D-glucose depends upon PKA activity.

Consistent with our findings in HFD animals, we found that phosphorylation of $\alpha 1_C$ at Ser^{1928} was significantly increased in arterial lysates prepared from diabetic compared to those from non-diabetic human subjects, without any change in total $Ca_V1.2$ protein abundance (Fig. 8A). We recorded single L-type Ca^{2+} channel activity in the cell-attached configuration from freshly isolated arterial myocytes from nondiabetic and diabetic human subjects. Cells from diabetic subjects had significantly enhanced L-type Ca^{2+} channel open probability (nP_o) (Fig. 8, B and C). Preincubation of the cells from diabetic subjects with rpcAMPS significantly reduced L-type Ca^{2+} channel nP_o to values similar to those observed in cells from nondiabetic patients (Fig. 8, B and C), suggesting that PKA plays a key role in stimulation of L-type Ca^{2+} channel activity during diabetes in human subjects. Together, our results are consistent with a mechanistic model whereby PKA activity determines phosphorylation of $\alpha 1_C$ at Ser^{1928}, leading to functional enhancement of L-type Ca^{2+} channel activity in human arterial myocytes in response to increased D-glucose and in diabetes.

DISCUSSION

Many studies have revealed impaired myogenic autoregulation that may contribute to increased vascular reactivity in the diabetic state (7). This has been associated, at least in part, with enhanced contractility of arterial myocytes in response to increased blood D-glucose (hyperglycemia) during diabetes (2–6). The mechanisms underlying this hypercontractility remain the subject of intense investigation, but links have been made to changes in PKC and Rho kinase signaling (52, 53), transcriptional remodeling due to activation of the prohypertensive transcription factor NFATc3 (3, 54), and reduced K^+ channel abundance and channel activity (3, 40, 55, 56). The results of the present study provide strong support for an additional model in which direct phosphorylation of $\alpha 1_C$ at Ser^{1928} by an AKAP150-anchored PKA plays a key role in stimulating Ca^{2+} influx through $Ca_V1.2$ channels, which leads to vasoconstriction during increases in extracellular glucose and in diabetes (Fig. 8D).

A central observation in this study was that increasing the concentration of glucose triggered an increase in global $[Ca^{2+}]_i$ in arterial myocytes, leading to vasoconstriction through a PKA-dependent pathway. These findings are paradoxical, because PKA activation plays a well-established role in arterial myocyte relaxation in response to endogenous and exogenous vasodilatory agents (57–61). Data reported here provide insight into this paradox by supporting a role for precise subsarcolemmal compartmentalization of a subpopulation of PKA in $Ca_V1.2$ channel regulation and vasoconstriction. Accordingly, targeting PKA to $Ca_V1.2$ channels by scaffolding proteins, such as AKAPs, may provide a means for selective phosphorylation of the channel to promote increased global Ca^{2+} and vasoconstriction rather than vasodilation. When PKA is tethered by an AKAP, dissociation of the catalytic subunit may not be required for substrate phosphorylation (62). Hence, association with the AKAP complex may be indispensable for spatial limitation of kinase activity within discrete cellular compartments. To extend the range of activity of an AKAP-anchored PKA, intrinsically disordered regions within RIIα subunits afford a high degree of flexibility within the anchored PKA holoenzyme, giving the catalytic subunits ~20-nm radius of motion. Considering the length of antibodies used to label proteins (~10 to 15 nm), the intermolecular distances between $Ca_V1.2$ and PKA_{cat} reported in the current study are conceivably within the limits required for selective modulation of $Ca_V1.2$ channel activity by PKA-mediated phosphorylation to promote contraction. In contrast, stimuli that induce cell-wide activation of PKA, such as forskolin, or activate a different PKA pool to stimulate other substrates, such as the phosphorylation of K^+ channels in response to β-adrenergic agonists (61, 63), may cause relaxation. Therefore, we predict that the spatial and temporal characteristics of the activated PKA signal determine the functional effects of PKA activity on vascular reactivity.

Another fundamental finding was that enhanced $Ca_V1.2$ channel activity in arterial myocytes in response to increases in extracellular D-glucose and in diabetes relies on phosphorylation of $\alpha 1_C$ at Ser^{1928}. This is a highly conserved residue among $\alpha 1_C$ subunits and is phosphorylated by PKA in response to various stimuli, such as β-adrenergic signals (17–21). Here, we showed that, in murine arterial myocytes and arteries, PKA-dependent phosphorylation of $\alpha 1_C$ at Ser^{1928} enhances vascular $Ca_V1.2$ channel activity and

vasoconstriction in response to increased extracellular D-glucose and in diabetic mice. Similar increases in PKA-mediated Ser^{1928} phosphorylation, $Ca_V1.2$ channel activity, and global Ca^{2+} signals were found in nondiabetic human arteries and myocytes in response to increasing the concentration of glucose and in arteries and myocytes from diabetic human subjects, thus highlighting the consistency of the results from the murine model with human pathology. In agreement with an important role for Ser^{1928}, we found that this single Ser-to-Ala substitution, which precludes phosphorylation of this site in S1928A knockin mice (21), prevented the enhancement in $Ca_V1.2$ channel activity and vasoconstriction in response to increased D-glucose. Moreover, enhanced $Ca_V1.2$ channel activity and myogenic tone in an HFD mouse model of diabetes were blocked in S1928A knockin mice on HFD, with no effect on basal $Ca_V1.2$ channel function. A reduction in K^+ channel function has also been proposed to promote membrane depolarization and vasoconstriction in response to acute increases in extracellular D-glucose (55, 56). Our data showing no functional impact of acute high glucose on arterial diameter in arteries from S1928A mice argue that direct phosphorylation of $\alpha 1_C$ at Ser^{1928}, leading to membrane potential–independent increase in $[Ca^{2+}]_i$, is required for enhanced vasoconstriction. However, this $Ca_V1.2$-dependent response could also act in concert with mechanisms of membrane potential dysregulation to exacerbate vascular tone in diabetes.

The essential influence of Ser^{1928} on $Ca_V1.2$ channel activity during PKA signaling in arterial myocytes is conserved in neurons, as revealed by Qian *et al.* (64). However, this phosphorylation event does not seem to be important for PKA-dependent regulation of $Ca_V1.2$ channel activity in cardiac cells (21). β-Adrenergic stimulation of $Ca_V1.2$ channels in ventricular myocytes from S1928A mice was normal, suggesting that Ser^{1928} phosphorylation by PKA is not necessary for sympathetic stimulation of channel activity and contraction in murine hearts (21). In contrast, Qian *et al.* report that S1928A mice have impaired long-term potentiation and compromised β-adrenergic–mediated stimulation of $Ca_V1.2$ activity by PKA in neurons, demonstrating a key role for Ser^{1928} in β-adrenergic regulation of $Ca_V1.2$ channel activity and neuronal function (64). The molecular mechanisms underlying these marked tissue-specific differences are unclear but may involve functional heterogeneity among distinct tissue-specific channel splice variants, a unique phosphorylation profile of $\alpha 1_C$, posttranslational regulation of other interacting proteins at distinct sites, or differential interaction with or regulation by different scaffold proteins and accessory subunits.

Ser^{1928} can also be phosphorylated by PKC (65), and activation of PKC increases $Ca_V1.2$ channel activity in arterial myocytes (66, 67). Enhanced activity of this kinase has also been associated with increased $Ca_V1.2$ channel activity and vascular reactivity during hypertension (68). We speculate that increased $Ca_V1.2$ channel activity during hypertension could be attributed to PKC-dependent phosphorylation of the same target residue. Thus, Ser^{1928} could represent a point of convergence to regulate $Ca_V1.2$ channel function by diverse signaling pathways. Furthermore, this phosphorylation site may be a distinct critical site of action for signal transduction in arterial myocytes, as well as a potential therapeutic target to treat vascular complications in diabetes and perhaps other pathological conditions.

Our previous studies have demonstrated that AKAP150 is necessary for regulation of vascular $Ca_V1.2$ channel by receptor-stimulated signals, such as angiotensin II (37, 68). This potent vasoconstrictor acts on G_q-coupled AT1 receptors to stimulate phospholipase C, generate diacylglycerol, and activate PKC. AKAP150 associates with AT1 receptors (69), and binding of PKC to AKAP150 is necessary for both acute and chronic angiotensin II stimulation of vascular $Ca_V1.2$ channels (37). Here, we confirmed the importance of AKAP150-bound PKC in modulating $Ca_V1.2$ channel activity and vascular reactivity during angiotensin II signaling using the ΔC knockin mouse. We also discovered that anchored PKC was not necessary for enhanced $Ca_V1.2$ channel activity in response to increased D-glucose. In contrast, the AKAP150 mutant lacking the PKA-binding site (ΔA) failed to enhance D-glucose–mediated phosphorylation of $\alpha 1_C$ at Ser^{1928} to promote $Ca_V1.2$ channel activity. Although the upstream mechanisms by which an increase in extracellular D-glucose leads to activation of AKAP150-anchored PKA in arterial myocytes are unclear, research from several groups suggested that glucose might stimulate a $G\alpha_s$ signal (70, 71). This would activate adenylyl cyclase to produce cyclic adenosine 3′,5′-monophosphate (cAMP), which leads to cAMP-dependent activation of PKA. The incorporation of AKAP150 in this pathway may coordinate the clustering of specialized G protein (heterotrimeric guanine nucleotide–binding protein)–coupled receptors, G proteins, and the downstream effectors to enable the decoding of different stimuli.

The augmented Ca^{2+} influx observed in cells exposed to prolonged increases in extracellular D-glucose or cells from animals or humans with diabetes may also activate a prohypertensive transcriptional cascade involving calcineurin and NFATc3 (Fig. 8D) (54, 68, 72, 73). Consistent with this, NFATc3 signaling is activated in an HFD mouse model of diabetes through a process that requires AKAP150-anchored calcineurin and Ca^{2+} influx through $Ca_V1.2$ channels (3). However, the abundance of $Ca_V1.2$ in arteries from wild-type HFD mice (3) and humans with diabetes (Fig. 8A) is similar to that in arteries from the corresponding LFD mice and nondiabetic subjects. Yet, NFATc3 activation leads to selective reduction in BK_{Ca} β1 and $K_V2.1$ subunit abundance and function, which may further contribute to enhanced vascular tone during diabetes (3, 40). Thus, we propose that AKAP150-anchored PKA and phosphorylation of $\alpha 1_C$ at Ser^{1928}, leading to increased $Ca_V1.2$ channel activity during chronic increases in extracellular D-glucose and diabetes, may activate AKAP150-anchored calcineurin to promote NFATc3 nuclear accumulation, transcriptional changes, and vascular dysfunction. Findings of restored myogenic tone in S1928A HFD animals may reflect the absence of an effect of diabetes on PKA-mediated $Ca_V1.2$ channel stimulation and a normalization of the steady-state global $[Ca^{2+}]_i$ as well as minimization of K^+ channel remodeling and normalization of membrane potential regulation through prevention of downstream NFATc3-dependent signaling. Therefore, regulatory events that are independent of membrane potential (PKA-mediated potentiation of $Ca_V1.2$ channel activity) and those that are dependent on membrane potential (down-regulation of K^+ channel activity, leading to depolarization and further $Ca_V1.2$ channel activation) may both modulate arterial myocyte $[Ca^{2+}]_i$ and contractility during diabetes.

We found that $Ca_V1.2$ channel activity is higher in cells and arteries from HFD mice and human subjects with diabetes even when measurements were performed in the presence of normal low concentrations of D-glucose. These results are similar to those observed in

arterial myocytes from a dB/dB mouse model of diabetes (8). Both Navedo *et al.* (8) and we here found that these differences were eliminated by PKA inhibition, suggesting that increased $Ca_V1.2$ channel function is the result of higher PKA activity in cells from diabetic animals and human subjects, thus providing evidence for "molecular memory." At present, it is unclear whether this increase in PKA activity results from altered upstream signaling (for example, activity of adenylyl cyclase), impaired activity of a phosphodiesterase, or changes in PKA subunit abundance or regulation.

In summary, our data indicated that, upon an increase in extracellular glucose, phosphorylation of $\alpha 1_C$ at Ser^{1928} by AKAP-anchored PKA is essential for enhanced $Ca_V1.2$ channel activity and increased global $[Ca^{2+}]_i$. Because contractility of arterial myocytes depends upon changes in global $[Ca^{2+}]_i$, higher $Ca_V1.2$ channel open probability in response to increased glucose and during diabetes may stimulate vasoconstriction in the resistance vasculature. Thus, activation of this pathway may have profound implications for tissue perfusion and blood pressure regulation during chronic hyperglycemia and diabetes.

MATERIALS AND METHODS

Animals

Male mice (5 to 8 weeks of age) were used for this study in strict accordance with protocols approved by the Animal Care and Use Committee of the University of California, Davis. In some experiments, mice were maintained on either an LFD (10% kcal) or HFD (60% kcal) (Research Diets) starting at 5 weeks of age for 12 to 16 weeks. The composition of these diets and the propensity of mice maintained on this HFD to develop type 2 diabetes and induce vascular dysfunction of small resistance arteries have been well documented in other studies (3, 50, 74). Wild-type (C57BL/6J), *AKAP150*$^{-/-}$ (C57BL/6J), and knockin mice expressing AKAP150 lacking its PKA RII binding site (ΔA; C57BL/6J) or PKC (ΔC; C57BL/6J) or in which Ser^{1928} of $\alpha 1_C$ was mutated to Ala (S1928A) were euthanized by intraperitoneal injection of sodium pentobarbital (250 mg/kg). Pial cerebral arteries were acutely dissected, and arterial myocytes were isolated using enzymatic digestion techniques as described (3, 75). For some experiments, third-order mesenteric and femoral arteries were isolated, and arterial myocytes were dissociated following the procedure above. Arteries and arterial myocytes were maintained in ice-cold nominally Ca^{2+}-free Ringer's solution (5 mM KCl, 140 mM NaCl, 2 mM $MgCl_2$, 10 mM Hepes, and 10 mM D-glucose adjusted to pH 7.4 with NaOH) containing normal 10 mM D-glucose until use.

Human arteries and cells

Excised human arteries from surgical patients undergoing gastric bypass procedure were obtained after institutional review board (IRB) approval and written consent and in accordance with the guidelines of the Declaration of Helsinki. Because our IRB exemption requires the use of noncoded tissue, a detailed therapeutic profile of the patient is unknown. Available patient information is included in table S3. Tissue was collected and placed in cold phosphate-buffered saline (PBS) solution containing normal D-glucose [138 mM NaCl, 3 mM KCl, 10 mM Na_2HPO_4, 2 mM NaH_2PO_4, 5 mM D-glucose, 0.1 mM $CaCl_2$, and 0.1 mM $MgSO_4$ (pH adjusted to 7.4)] and transferred to the laboratory. Small-diameter (~150- to

250-μm-diameter) arteries were carefully dissected out of surrounding tissue and used for experimentation. Arterial myocytes were enzymatically isolated using a two-step digestion process as described (3, 75). Cells were maintained in ice-cold nominally Ca^{2+}-free Ringer's solution with normal D-glucose concentration (5 mM) until use.

Immunolabeling and STORM

Isolated arterial myocytes were allowed to adhere to a coverslip before fixing with PBS containing 3% paraformaldehyde + 0.1% glutaraldehyde followed by 0.1% sodium borohydride. After washing with PBS, cells were permeabilized and blocked with 0.5% Triton X-100 and 3% bovine serum albumin and exposed overnight to custom antibody against $Ca_V1.2$ (28, 76) and antibody against PKA_{cat} α, β, γ (Santa Cruz Biotechnology). For secondary antibodies, we used a goat FLIP 565–conjugated antibody recognizing rabbit immunoglobulin G (IgG) and goat Alexa Fluor 647–conjugated antibody recognizing mouse IgG. The specificity of secondary antibodies to detect corresponding primary antibodies was tested in control experiments in which cells were only treated with secondary antibodies before imaging (−1° antibody control). We used a Nikon N-STORM super-resolution microscope system to capture images after TIRF illumination with 561- and 640-nm laser light. During imaging, cells were bathed in PBS (pH 7.4) containing glucose oxidase (0.56 mg/ml), catalase (0.3 mg/ml), and cysteamine (10mM). Aseries of 20,000 images were acquired using a Plan Apochromat TIRF 100× oil immersion lens [numerical aperture (NA), 1.49] and an iXon3 DU-897E electron-multiplying charge-coupled device (EMCCD) camera (Andor Technology). STORM images were rendered by plotting molecule localization as a Gaussian that was proportional to the number of photons released per photoswitching event. The full width at half maximum measured for single-molecule signals was ~31 nm. Reconstructions were filtered to reject localizations generated from less than 600 photons or from events that were detected on eight or greater consecutive frames. Half-maximal intensity for single molecules in reconstructed images was used to set a threshold for binary analysis, and the shortest intermolecular distance was determined for $Ca_V1.2$ and PKA_{cat} using the JACoP plug-in of ImageJ software [National Institutes of Health (NIH)] as before (77, 78). Intermolecular distance histograms were fit with a sum of two Gaussian functions of the following equation: $Y = A \times \exp(-0.5((X - \text{Mean}_1)/\sigma_1)^2) + B \times \exp(-0.5((X - \text{Mean}_2)/\sigma_2)^2)$, where A and B are the heights of the center of the distribution of distances expressed as a percentage of total points, Mean_1 and Mean_2 are the x values of distance at the center of the two distributions, and σ_1 and σ_2 are the widths of each distribution in nanometers.

Structured illumination microscopy

Arterial myocytes were fixed, permeabilized, blocked, and incubated with primary antibodies against $Ca_V1.2$ and PKA_{cat} as described above. Goat Alexa Fluor 488–conjugated antibody against rabbit and goat Alexa Fluor 568–conjugated antibody against mouse were used as secondary antibodies. Images were captured using a Nikon N-SIM microscopy system coupled to a Nikon ECLIPSE Ti-E inverted microscope. The specimen was illuminated with 488- and 561-nm laser light by high-frequency patterned illumination. Images were captured at a focal plan at the z-axis center of an arterial myocyte using a CFI SR Apochromat TIRF 100× oil immersion lens and an iXon3 DU-897E EMCCD camera

(Andor Technology). Cellular protein ultrastructure was determined by reconstruction using a computer algorithm in Nikon Elements AR software. The percent of total $Ca_V1.2$-associated centroids within 100 nm to the nearest PKA_{cat}-associated centroids was determined using the JACoP plug-in of ImageJ software (NIH) as described above.

Immunofluorescence

Immunofluorescence labeling of freshly isolated arterial myocytes was performed as described (37) using a monoclonal antibody against $Ca_V1.2$ (NeuroMab, clone N263/31; 1:1000) and TfR (Thermo Scientific, clone H68.4; 1:1000) and goat antibody against ANO1 (Santa Cruz Biotechnology, clone S-20; 1:1000). The secondary antibody was either a donkey Alexa Fluor 568–conjugated antibody against mouse (5 mg/ml) or donkey Alexa Fluor 568–conjugated antibody against goat (5 mg/ml) from Molecular Probes. Cells were imaged (512 × 512–pixel images) using an Olympus FV1000 confocal microscope coupled with an Olympus 60× water immersion lens (NA, 1.2) and a zoom of 3.0 (pixel size, 0.138 μm). Images were collected at multiple optical planes (*z*-axis step size, 0.35 μm). The specificity of the primary antibody was tested in negative control experiments in which the primary antibody was substituted with PBS. $Ca_V1.2$-, TfR-, and ANO1-associated fluorescence was not detected under this experimental condition. The same laser power, gain settings, and pinhole were used to image arterial myocytes under different experimental conditions.

Proximity ligation assay

A Duolink In Situ PLA kit was used to detect complexes consisting of $Ca_V1.2$ and PKA_{cat} in freshly dissociated arterial myocytes. Cells were plated on glass coverslips and allowed to adhere (30 min, room temperature) before fixing with 4% paraformaldehyde (20 min), quenching in 100 mM glycine (15 min), and washing in PBS (2 × 3 min). Cells were then permeabilized with 0.1% Triton X-100 (20 min) and blocked (1 hour, 37°C) in 50% Odyssey blocking solution (LI-COR Biosciences). Cells were incubated overnight with a specific combination of primary antibodies [mouse antibody against PKA_{cat} (Santa Cruz Biotechnology, sc-365615, 1:1000), custom rabbit antibody specific for $Ca_V1.2$ (1:1000) (28, 76), monoclonal antibody specific for $Ca_V1.2$ (NeuroMab, clone N263/31 AB_11000167, 1:1000) and TfR (Thermo Scientific, clone H68.4, #13-6800, 1:1000), and goat antibody against ANO1 (Santa Cruz Biotechnology, clone S-20, sc-69343, 1:1000)] in Duolink antibody diluent solution. As a control, cells were incubated with only one primary antibody. Secondary antibodies conjugated with oligonucleotides (PLA probes, antibody against rabbit PLUS and antibody against mouse MINUS) were used to detect $Ca_V1.2$ and PKA, $Ca_V1.2$ and TfR, and $Ca_V1.2$ and ANO1 (1 hour, 37°C). After incubation with probes, a ligation solution consisting of two distinct oligonucleotides and ligase was added and incubated for 30 min at 37°C to allow hybridization and formation of a circular DNA template at sites of dual labeling. The ligation step is followed by a rolling circle amplification reaction (100 min, 37°C) using the ligated circle as a template. The ligation reaction was followed by washing in Duolink buffer B (2 × 10 min) and in 1% buffer B (1 × 1 min). Coverslips were allowed to dry and subsequently mounted on a microscope slide with Duolink mounting medium. The fluorescence signal was visualized using an Olympus FV1000 confocal microscopy system on an Olympus IX81 microscope with a 60× oil

immersion lens (NA, 1.54). Images were acquired at different optical planes (*z*-axis step size, 0.5 μm). The stack of images for each sample was then combined into a single-intensity projection image that was subsequently used for analysis of number of puncta per square micrometer per cell. For presentation, representative PLA images at the center of the *z* axis are shown. Before labeled specimens were imaged, photomultiplier gain and laser power parameters were determined using control cells in which primary antibodies were omitted. Images for all conditions were obtained using the same acquisition parameters.

Electrophysiology

Freshly isolated arterial myocytes were allowed to adhere to a glass coverslip in a recording chamber for 10 min. $Ca_V1.2$ channel activity was examined using the perforated whole-cell patch-clamp technique to record macroscopic currents with Ba^{2+} as a charge carrier. The pipette solution contained 120 mM CsCl, 20 mM tetraethylammonium chloride (TEA-Cl), 1 mM EGTA, and 20 mM Hepes with amphotericin B (250 μg/ml; pH adjusted to 7.2 with CsOH). Cells were bathed in a solution containing 115 mM NaCl, 10 mM TEA-Cl, 0.5 mM $MgCl_2$, 10 mM D-glucose, 5 mM CsCl, 20 mM $BaCl_2$, and 20 mM Hepes (pH adjusted to 7.4 with CsOH). All electrophysiological experiments were performed at 21° to 23°C. Experiments were terminated by application of the experimental solution containing 1 μM nifedipine to determine the nifedipine-sensitive component, which is produced by $Ca_V1.2$ channels containing $\alpha 1_C$ subunits. To obtain the *I-V* relationship of nifedipine-sensitive Ba^{2+} currents, we depolarized cells for 200 ms from the holding potential of −70 mV to voltages ranging from −60 to +60 mV. The *I-V* relationship for averaged data sets was fit with a peak Gaussian function: $I(V) = I_{max} \times \exp(-0.5((V - V_{max})/b)^2)$, where I_{max} is peak I, V_{max} is V at I_{max}, and b is the slope of the distribution, as described previously (79).

Single-channel Ca^{2+} currents were recorded from arterial myocytes in the cell-attached configuration of the patch-clamp technique as described (80–82). Briefly, data were acquired at a sampling rate of 50 μs and low pass–filtered at 2 kHz with an Axopatch 200B amplifier and Digidata 1440 digitizer (Molecular Devices). Data were subsequently filtered with a Gaussian filter (400 Hz) during analysis. Pipettes were pulled from borosilicate capillary glass using a micropipette puller (model P-97, Sutter Instruments). Pipettes were polished to achieve resistances that range from 3.5 to 6.5 megohms. The pipette solution contained 120 mM TEA-Cl, 110 mM $CaCl_2$, and 10 mM Hepes. BayK-8644 (500 nM) was included in the pipette solution to promote longer open times, thereby facilitating measurement of small unitary L-type Ca^{2+} currents and increasing the probability of sweeps with channel activity. Bath solution contained 145 mM KCl, 10 mM NaCl, and 10 mM Hepes [pH 7.4 (NaOH)]. This high K^+ solution was used to fix the membrane resting potential to ~0 mV (83, 84). L-type Ca^{2+} currents were evoked by a 2-s step depolarization to −30 mV from the holding potential of −70 mV. Capacitive currents were compensated by subtraction of blank sweeps. Single-channel events were recorded using the Axopatch module of the pCLAMP 10 software. $Ca_V1.2$ channel activity was negligible when nifedipine was included in the patch pipette. The single-channel event half-amplitude detection algorithm from pCLAMP 10 was used to analyze single-channel openings and nP_o. The unitary channel amplitude in our single-channel recordings is ~0.53 pA, which corresponds to the expected single-channel

activity for $Ca_V1.2$ channels under our experimental conditions (81, 85). All experiments were performed at room temperature.

Arterial diameter measurements

Freshly isolated posterior cerebral arteries were cannulated on glass micropipettes mounted in a 5-ml myograph chamber (University of Vermont Instrumentation and Model Facility) as described (86). For some experiments, endothelial function was ablated by passing an air bubble through the lumen during the cannulation procedure. To allow for equilibration, arteries were pressurized to 20 mmHg and continuously perfused (37°C, 30 min, 3 to 5 ml/min) with physiological saline solution consisting of 119 mM NaCl, 4.7 mM KCl, 2 mM $CaCl_2$, 24 mM $NaHCO_3$, 1.2 mM KH_2PO_4, 1.2 mM $MgSO_4$, 0.023 mM EDTA, and 10 mM D-glucose aerated with 5% CO_2/95% O_2. Bath pH was closely monitored and maintained at 7.35 to 7.4. After equilibration period, intravascular pressure was increased and arteries were allowed to develop myogenic tone. Arteries not exhibiting stable myogenic tone after ~1 hour were discarded. To assess the response of arterial diameter to hyperglycemic conditions in pressurized vessels, D-glucose was increased in the perfusion solution from 10 to 20 mM. Arterial tone data are presented as a percent decrease in diameter relative to the maximum passive diameter at a given intravascular pressure obtained at the end of each experiment using Ca^{2+}-free saline solution containing 1 μM nifedipine.

$[Ca^{2+}]_i$ measurements

Global cell-wide $[Ca^{2+}]_i$ was recorded as described (8). Briefly, global cytosolic $[Ca^{2+}]_i$ was imaged in isolated arterial smooth muscle cells loaded with the membrane-permeable acetoxymethyl ester Fluo-4 (15 min, room temperature). Cells were bathed in a Hepes-buffered saline solution containing 140 mM NaCl, 5 mM KCl, 1 mM $MgCl_2$, 2 mM $CaCl_2$, 10 mM Hepes, and 10 or 20 mM D-glucose. Images were collected using an Andor spinning disk confocal system coupled to an Olympus iX-81 inverted microscope equipped with an Olympus 60× oil immersion lens (NA, 1.49). Background-subtracted images were normalized by dividing the fluorescence intensity of each pixel (F) by the average resting fluorescence intensity (F_o) of a confocal image to determine the F/F_o-time relationship.

Immunoprecipitation and immunoblotting

Whole lysates were obtained from cerebral and mesenteric arteries by sonication (20 min, 4°C) in lysis buffer solution containing 150 mM NaCl, 10 mM Na_2HPO_4, and 1 mM EDTA with 1% deoxycholic acid, 0.1% SDS, and protease inhibitors (cOmplete Mini Protease Inhibitor Cocktail, Roche) with 2 μM microcystin and 1 mM *p*-nitrophenyl phosphate to inhibit endogenous phosphatase activity. Samples were cleared from nonsolubilized material by ultracentrifugation (250,000*g* for 30 min) before immunoprecipitation (4 hours, 4°C) with an antibody against $Ca_V1.2$ [4 μg of FP1 (28)] using protein A–Sepharose. An equal amount of nonspecific rabbit IgG was used as control for immunoprecipitation. Beads were washed three times with washing buffer [150 mM NaCl, 10 mM EDTA, 10 mM EGTA, 10 mM tris-HCl, 0.1% Triton X-100 (pH 7.4)]. Samples were boiled in Laemmli Sample Buffer (Bio-Rad) for 5 min at 95°C and run on an ~8% acrylamide gel in SDS–polyacrylamide gel electrophoresis before they were transferred onto polyvinylidene difluoride membranes. Membranes were blocked in blocking solution [5% dry milk in tris-buffered saline (TBS)

containing 0.05% Tween 20] before incubation with primary antibodies (blocking solution for 1 hour) followed by three 15-min washes in TBS with 0.05% Tween 20, incubation with horseradish peroxidase (HRP)–protein A (1:10,000 in blocking solution for 1 hour), several washes for 2 hours, and detection of HRP with enhanced chemiluminescence (ECL), ECL Plus, or Femto chemiluminescence reagents. Primary antibodies were from Santa Cruz Biotechnology (α-tubulin, sc-32293), BD Transduction Laboratories (PKA-RIIα, #612242), EMD Millipore (AKAP150, #07210), NeuroMab (K_V2.1, clone K89/34), Alomone (BK_{Ca} α, APC-021), Abcam (BK_{Ca} β1, ab3587), and Cell Signaling Technology (PKCα). Multiple exposures with increasing time periods were obtained to ensure that signals were in the linear range, as described (17, 34).

Chemicals and statistical analyses

All chemical reagents were from Sigma-Aldrich unless otherwise stated. Data are expressed as means ± SEM. Data were analyzed using GraphPad Prism software. Statistical significance was determined using appropriate paired or unpaired Student's *t* test, ANOVA, or nonparametric tests. Statistical significance, denoted by asterisk in figures, was considered at $P < 0.05$.

Supplementary Material

Refer to Web version on PubMed Central for supplementary material.

Acknowledgments

We thank K. Johnson for technical support. **Funding:** This work was supported by NIH grants R01-HL098200 and R01-HL121059 and American Heart Association grant 14GRNT18730054 (to M.F.N.), NIH grant P20-GM103492 and American Heart Association grants 13POST12730001 and 16SDG27260070 (to M.A.N.), NIH grant T32-GM099608 (to M.P.P.), NIH grants R01-DK54441 and R01-DK105542 (to J.D.S.), NIH grant R01-DK057236 (to S.M.W.), and NIH grants R01-MH097887 and R01-NS078792 (to J.W.H.). J.D.S. is an investigator of the Howard Hughes Medical Institute.

REFERENCES AND NOTES

1. National High Blood Pressure Education Program Working Group report on hypertension in diabetes. Hypertension. 1994; 23:145–158. [PubMed: 8307622]
2. Barbagallo M, Shan J, Pang PK, Resnick LM. Glucose-induced alterations of cytosolic free calcium in cultured rat tail artery vascular smooth muscle cells. J. Clin. Invest. 1995; 95:763–767. [PubMed: 7860758]
3. Nystoriak MA, Nieves-Cintrón M, Nygren PJ, Hinke SA, Nichols CB, Chen C-Y, Puglisi JL, Izu LT, Bers DM, Dell'Acqua ML, Scott JD, Santana LF, Navedo MF. AKAP150 contributes to enhanced vascular tone by facilitating large-conductance Ca^{2+}–activated K^+ channel remodeling in hyperglycemia and diabetes mellitus. Circ. Res. 2014; 114:607–615. [PubMed: 24323672]
4. Ungvari Z, Pacher P, Kecskemeti V, Papp G, Szollár L, Koller A. Increased myogenic tone in skeletal muscle arterioles of diabetic rats. Possible role of increased activity of smooth muscle Ca^{2+} channels and protein kinase C. Cardiovasc. Res. 1999; 43:1018–1028. [PubMed: 10615429]
5. Brown A, Reynolds LR, Bruemmer D. Intensive glycemic control and cardiovascular disease: An update. Nat. Rev. Cardiol. 2010; 7:369–375. [PubMed: 20404853]
6. Fleischhacker E, Esenabhalu VE, Spitaler M, Holzmann S, Skrabal F, Koidl B, Kostner GM, Graier WF. Human diabetes is associated with hyperreactivity of vascular smooth muscle cells due to altered subcellular Ca^{2+} distribution. Diabetes. 1999; 48:1323–1330. [PubMed: 10342823]

7. Cooper ME, Bonnet F, Oldfield M, Jandeleit-Dahm K. Mechanisms of diabetic vasculopathy: An overview. Am. J. Hypertens. 2001; 14:475–486. [PubMed: 11368471]
8. Navedo MF, Takeda Y, Nieves-Cintrón M, Molkentin JD, Santana LF. Elevated Ca^{2+} sparklet activity during acute hyperglycemia and diabetes in cerebral arterial smooth muscle cells. Am. J. Physiol. Cell Physiol. 2010; 298:C211–C220. [PubMed: 19846755]
9. Hofmann F, Flockerzi V, Kahl S, Wegener JW. L-type $Ca_V1.2$ calcium channels: From in vitro findings to in vivo function. Physiol. Rev. 2014; 94:303–326. [PubMed: 24382889]
10. Navedo MF, Santana LF. $Ca_V1.2$ sparklets in heart and vascular smooth muscle. J. Mol. Cell. Cardiol. 2013; 58:67–76. [PubMed: 23220157]
11. Catterall WA. Structure and regulation of voltage-gated Ca^{2+} channels. Annu. Rev. Cell Dev. Biol. 2000; 16:521–555. [PubMed: 11031246]
12. Keef KD, Hume JR, Zhong J. Regulation of cardiac and smooth muscle Ca^{2+} channels ($Ca_V1.2a,b$) by protein kinases. Am. J. Physiol. Cell Physiol. 2001; 281:C1743–C1756. [PubMed: 11698232]
13. Ishikawa T, Hume JR, Keef KD. Regulation of Ca^{2+} channels by cAMP and cGMP in vascular smooth muscle cells. Circ. Res. 1993; 73:1128–1137. [PubMed: 8222084]
14. Zhong J, Hume JR, Keef KD. Anchoring protein is required for cAMP-dependent stimulation of L-type Ca^{2+} channels in rabbit portal vein. Am. J. Physiol. 1999; 277:C840–C844. [PubMed: 10516114]
15. Navedo MF, Amberg GC. Local regulation of L-type Ca^{2+} channel sparklets in arterial smooth muscle. Microcirculation. 2013; 20:290–298. [PubMed: 23116449]
16. Dai S, Hall DD, Hell JW. Supramolecular assemblies and localized regulation of voltage-gated ion channels. Physiol. Rev. 2009; 89:411–452. [PubMed: 19342611]
17. Davare MA, Hell JW. Increased phosphorylation of the neuronal L-type Ca^{2+} channel $Ca_V1.2$ during aging. Proc. Natl. Acad. Sci. U.S.A. 2003; 100:16018–16023. [PubMed: 14665691]
18. De Jongh KS, Murphy BJ, Colvin AA, Hell JW, Takahashi M, Catterall WA. Specific phosphorylation of a site in the full-length form of the α1 subunit of the cardiac L-type calcium channel by adenosine 3′,5′- cyclic monophosphate-dependent protein kinase. Biochemistry. 1996; 35:10392–10402. [PubMed: 8756695]
19. Hulme JT, Westenbroek RE, Scheuer T, Catterall WA. Phosphorylation of serine 1928 in the distal C-terminal domain of cardiac $Ca_V1.2$ channels during β1-adrenergic regulation. Proc. Natl. Acad. Sci. U.S.A. 2006; 103:16574–16579. [PubMed: 17053072]
20. Murphy JG, Sanderson JL, Gorski JA, Scott JD, Catterall WA, Sather WA, Dell'Acqua ML. AKAP-anchored PKA maintains neuronal L-type calcium channel activity and NFAT transcriptional signaling. Cell Rep. 2014; 7:1577–1588. [PubMed: 24835999]
21. Lemke T, Welling A, Christel CJ, Blaich A, Bernhard D, Lenhardt P, Hofmann F, Moosmang S. Unchanged β-adrenergic stimulation of cardiac L-type calcium channels in $Ca_V1.2$ phosphorylation site S1928A mutant mice. J. Biol. Chem. 2008; 283:34738–34744. [PubMed: 18829456]
22. Ganesan AN, Maack C, Johns DC, Sidor A, O'Rourke B. β-Adrenergic stimulation of L-type Ca^{2+} channels in cardiac myocytes requires the distal carboxyl terminus of α_{1C} but not serine 1928. Circ. Res. 2006; 98:e11–e18. [PubMed: 16397147]
23. Fuller MD, Emrick MA, Sadilek M, Scheuer T, Catterall WA. Molecular mechanism of calcium channel regulation in the fight-or-flight response. Sci. Signal. 2010; 3:ra70. [PubMed: 20876873]
24. Gao T, Yatani A, Dell'Acqua ML, Sako H, Green SA, Dascal N, Scott JD, Hosey MM. cAMP-dependent regulation of cardiac L-type Ca^{2+} channels requires membrane targeting of PKA and phosphorylation of channel subunits. Neuron. 1997; 19:185–196. [PubMed: 9247274]
25. Jones BW, Brunet S, Gilbert ML, Nichols CB, Su T, Westenbroek RE, Scott JD, Catterall WA, McKnight GS. Cardiomyocytes from AKAP7 knockout mice respond normally to adrenergic stimulation. Proc. Natl. Acad. Sci. U.S.A. 2012; 109:17099–17104. [PubMed: 23035250]
26. Hall DD, Davare MA, Shi M, Allen ML, Weisenhaus M, McKnight GS, Hell JW. Critical role of cAMP-dependent protein kinase anchoring to the L-type calcium channel $Ca_V1.2$ via A-kinase anchor protein 150 in neurons. Biochemistry. 2007; 46:1635–1646. [PubMed: 17279627]

27. Oliveria SF, Dell'Acqua ML, Sather WA. AKAP79/150 anchoring of calcineurin controls neuronal L-type Ca^{2+} channel activity and nuclear signaling. Neuron. 2007; 55:261–275. [PubMed: 17640527]
28. Davare MA, Horne MC, Hell JW. Protein phosphatase 2A is associated with class C L-type calcium channels ($Ca_V1.2$) and antagonizes channel phosphorylation by cAMP-dependent protein kinase. J. Biol. Chem. 2000; 275:39710–39717. [PubMed: 10984483]
29. Fredriksson S, Gullberg M, Jarvius J, Olsson C, Pietras K, Gústafsdóttir SM, Östman A, Landegren U. Protein detection using proximity-dependent DNA ligation assays. Nat. Biotechnol. 2002; 20:473–477. [PubMed: 11981560]
30. Schweizer A, Fransen JA, Bächi T, Ginsel L, Hauri HP. Identification, by a monoclonal antibody, of a 53-kD protein associated with a tubulo-vesicular compartment at the cis-side of the Golgi apparatus. J. Cell Biol. 1988; 107:1643–1653. [PubMed: 3182932]
31. Vollenweider F, Kappeler F, Itin C, Hauri H-P. Mistargeting of the lectin ERGIC-53 to the endoplasmic reticulum of HeLa cells impairs the secretion of a lysosomal enzyme. J. Cell Biol. 1998; 142:377–389. [PubMed: 9679138]
32. Di Biase V, Tuluc P, Campiglio M, Obermair GJ, Heine M, Flucher BE. Surface traffic of dendritic $Ca_V1.2$ calcium channels in hippocampal neurons. J. Neurosci. 2011; 31:13682–13694. [PubMed: 21940459]
33. Jin X, Shah S, Liu Y, Zhang H, Lees M, Fu Z, Lippiat JD, Beech DJ, Sivaprasadarao A, Baldwin SA, Zhang H, Gamper N. Activation of the Cl^- channel ANO1 by localized calcium signals in nociceptive sensory neurons requires coupling with the IP_3 receptor. Sci. Signal. 2013; 6:ra73. [PubMed: 23982204]
34. Hall DD, Feekes JA, Don A. S. Arachchige, Shi M, Hamid J, Chen L, Strack S, Zamponi GW, Horne MC, Hell JW. Binding of protein phosphatase 2A to the L-type calcium channel $Ca_V1.2$ next to Ser1928, its main PKA site, is critical for Ser1928 dephosphorylation. Biochemistry. 2006; 45:3448–3459. [PubMed: 16519540]
35. Faux MC, Rollins EN, Edwards AS, Langeberg LK, Newton AC, Scott JD. Mechanism of A-kinase-anchoring protein 79 (AKAP79) and protein kinase C interaction. Biochem. J. 1999; 343:443–452. [PubMed: 10510312]
36. Hoshi N, Langeberg LK, Scott JD. Distinct enzyme combinations in AKAP signalling complexes permit functional diversity. Nat. Cell Biol. 2005; 7:1066–1073. [PubMed: 16228013]
37. Navedo MF, Nieves-Cintrón M, Amberg GC, Yuan C, Votaw VS, Lederer WJ, McKnight GS, Santana LF. AKAP150 is required for stuttering persistent Ca^{2+} sparklets and angiotensin II-induced hypertension. Circ. Res. 2008; 102:e1–e11. [PubMed: 18174462]
38. Nichols CB, Rossow CF, Navedo MF, Westenbroek RE, Catterall WA, Santana LF, McKnight GS. Sympathetic stimulation of adult cardiomyocytes requires association of AKAP5 with a subpopulation of L-type calcium channels. Circ. Res. 2010; 107:747–756. [PubMed: 20671242]
39. Gustafsson MGL. Surpassing the lateral resolution limit by a factor of two using structured illumination microscopy. J. Microsc. 2000; 198:82–87. [PubMed: 10810003]
40. Nieves-Cintrón M, Nystoriak MA, Prada MP, Johnson K, Fayer W, Dell'Acqua ML, Scott JD, Navedo MF. Selective downregulation of $K_V2.1$ function contributes to enhanced arterial tone during diabetes. J. Biol. Chem. 2015; 290:7918–7929. [PubMed: 25670860]
41. Park JL, Loberg RD, Duquaine D, Zhang H, Deo BK, Ardanaz N, Coyle J, Atkins KB, Schin M, Charron MJ, Kumagai AK, Pagano PJ, Brosius FC III. GLUT4 facilitative glucose transporter specifically and differentially contributes to agonist-induced vascular reactivity in mouse aorta. Arterioscler. Thromb. Vasc. Biol. 2005; 25:1596–1602. [PubMed: 15890973]
42. Davare MA, Dong F, Rubin CS, Hell JW. The A-kinase anchor protein MAP2B and cAMP-dependent protein kinase are associated with class C L-type calcium channels in neurons. J. Biol. Chem. 1999; 274:30280–30287. [PubMed: 10514522]
43. Brayden JE, Nelson MT. Regulation of arterial tone by activation of calcium-dependent potassium channels. Science. 1992; 256:532–535. [PubMed: 1373909]
44. Knot HJ, Nelson MT. Regulation of membrane potential and diameter by voltage-dependent K^+ channels in rabbit myogenic cerebral arteries. Am. J. Physiol. 1995; 269:H348–H355. [PubMed: 7631867]

45. Amberg GC, Santana LF. Kv2 channels oppose myogenic constriction of rat cerebral arteries. Am. J. Physiol. Cell Physiol. 2006; 291:C348–C356. [PubMed: 16571867]
46. Nelson MT, Quayle JM. Physiological roles and properties of potassium channels in arterial smooth muscle. Am. J. Physiol. 1995; 268:C799–C822. [PubMed: 7733230]
47. Erickson JR, Pereira L, Wang L, Han G, Ferguson A, Dao K, Copeland RJ, Despa F, Hart GW, Ripplinger CM, Bers DM. Diabetic hyperglycaemia activates CaMKII and arrhythmias by O-linked glycosylation. Nature. 2013; 502:372–376. [PubMed: 24077098]
48. Vaidyanathan K, Wells L. Multiple tissue-specific roles for the *O*-GlcNAc post-translational modification in the induction of and complications arising from type II diabetes. J. Biol. Chem. 2014; 289:34466–34471. [PubMed: 25336652]
49. Surwit RS, Kuhn CM, Cochrane C, McCubbin JA, Feinglos MN. Diet-induced type II diabetes in C57BL/6J mice. Diabetes. 1988; 37:1163–1167. [PubMed: 3044882]
50. Winzell MS, Ahrén B. The high-fat diet–fed mouse: A model for studying mechanisms and treatment of impaired glucose tolerance and type 2 diabetes. Diabetes. 2004; 53(suppl. 3):S215–S219. [PubMed: 15561913]
51. Knot HJ, Nelson MT. Regulation of arterial diameter and wall [Ca^{2+}] in cerebral arteries of rat by membrane potential and intravascular pressure. J. Physiol. 1998; 508:199–209. [PubMed: 9490839]
52. Hien TT, Turczyńska KM, Dahan D, Ekman M, Grossi M, Sjögren J, Nilsson J, Braun T, Boettger T, Garcia-Vaz E, Stenkula K, Swärd K, Gomez MF, Albinsson S. Elevated glucose levels promote contractile and cytoskeletal gene expression in vascular smooth muscle via rho/protein kinase C and actin polymerization. J. Biol. Chem. 2016; 291:3552–3568. [PubMed: 26683376]
53. Kizub IV, Pavlova OO, Johnson CD, Soloviev AI, Zholos AV. Rho kinase and protein kinase C involvement in vascular smooth muscle myofilament calcium sensitization in arteries from diabetic rats. Br. J. Pharmacol. 2010; 159:1724–1731. [PubMed: 20218979]
54. Nilsson J, Nilsson LM, Chen Y-W, Molkentin JD, Erlinge D, Gomez MF. High glucose activates nuclear factor of activated T cells in native vascular smooth muscle. Arterioscler. Thromb. Vasc. Biol. 2006; 26:794–800. [PubMed: 16469950]
55. Straub SV, Girouard H, Doetsch PE, Hannah RM, Wilkerson MK, Nelson MT. Regulation of intracerebral arteriolar tone by K_V channels: Effects of glucose and PKC. Am. J. Physiol. Cell Physiol. 2009; 297:C788–C796. [PubMed: 19605735]
56. Rainbow RD, Hardy MEL, Standen NB, Davies NW. Glucose reduces endothelin inhibition of voltage-gated potassium channels in rat arterial smooth muscle cells. J. Physiol. 2006; 575:833–844. [PubMed: 16825302]
57. Porter VA, Bonev AD, Knot HJ, Heppner TJ, Stevenson AS, Kleppisch T, Lederer WJ, Nelson MT. Frequency modulation of Ca^{2+} sparks is involved in regulation of arterial diameter by cyclic nucleotides. Am. J. Physiol. 1998; 274:C1346–C1355. [PubMed: 9612222]
58. Wellman GC, Santana LF, Bonev AD, Nelson MT. Role of phospholamban in the modulation of arterial Ca^{2+} sparks and Ca^{2+}-activated K^+ channels by cAMP. Am. J. Physiol. Cell Physiol. 2001; 281:C1029–C1037. [PubMed: 11502581]
59. Wellman GC, Bonev AD, Nelson MT, Brayden JE. Gender differences in coronary artery diameter involve estrogen, nitric oxide, and Ca^{2+}-dependent K^+ channels. Circ. Res. 1996; 79:1024–1030. [PubMed: 8888695]
60. Aiello EA, Walsh MP, Cole WC. Phosphorylation by protein kinase A enhances delayed rectifier K^+ current in rabbit vascular smooth muscle cells. Am. J. Physiol. 1995; 268:H926–H934. [PubMed: 7864221]
61. Moore CL, Nelson PL, Parelkar NK, Rusch NJ, Rhee SW. Protein kinase A–phosphorylated K_V1 channels in PSD95 signaling complex contribute to the resting membrane potential and diameter of cerebral arteries. Circ. Res. 2014; 114:1258–1267. [PubMed: 24585759]
62. Smith FD, Reichow SL, Esseltine JL, Shi D, Langeberg LK, Scott JD, Gonen T. Intrinsic disorder within an AKAP-protein kinase A complex guides local substrate phosphorylation. eLife. 2013; 2:e01319. [PubMed: 24192038]

63. Li H, Chai Q, Gutterman DD, Liu Y. Elevated glucose impairs cAMP-mediated dilation by reducing K_V channel activity in rat small coronary smooth muscle cells. Am. J. Physiol. Heart Circ. Physiol. 2003; 285:H1213–H1219. [PubMed: 12763748]
64. Qian H, Patriarchi T, Price JL, Matt L, Buonarati OR, Chowdhury D, Nanou E, Nystoriak MA, Catterall WA, Poomvanicha M, Hofmann F, Navedo MF, Hell JW. Phosphorylation of Ser^{1928} mediates the enhanced activity of the L-type Ca^{2+} channel $Ca_V1.2$ by the β_2-adrenergic receptor in neurons. Sci. Signal. 2017; 10:eaaf9659. [PubMed: 28119465]
65. Yang L, Liu G, Zakharov SI, Morrow JP, Rybin VO, Steinberg SF, Marx SO. Ser^{1928} is a common site for $Ca_V1.2$ phosphorylation by protein kinase C isoforms. J. Biol. Chem. 2005; 280:207–214. [PubMed: 15509562]
66. Navedo MF, Amberg GC, Nieves M, Molkentin JD, Santana LF. Mechanisms underlying heterogeneous Ca^{2+} sparklet activity in arterial smooth muscle. J. Gen. Physiol. 2006; 127:611–622. [PubMed: 16702354]
67. Navedo MF, Amberg GC, Votaw VS, Santana LF. Constitutively active L-type Ca^{2+} channels. Proc. Natl. Acad. Sci. U.S.A. 2005; 102:11112–11117. [PubMed: 16040810]
68. Nieves-Cintrón M, Amberg GC, Navedo MF, Molkentin JD, Santana LF. The control of Ca^{2+} influx and NFATc3 signaling in arterial smooth muscle during hypertension. Proc. Natl. Acad. Sci. U.S.A. 2008; 105:15623–15628. [PubMed: 18832165]
69. Zhang J, Bal M, Bierbower S, Zaika O, Shapiro MS. AKAP79/150 signal complexes in G-protein modulation of neuronal ion channels. J. Neurosci. 2011; 31:7199–7211. [PubMed: 21562284]
70. Tamaki H. Glucose-stimulated cAMP-protein kinase a pathway in yeast *Saccharomyces cerevisiae*. J. Biosci. Bioeng. 2007; 104:245–250. [PubMed: 18023794]
71. Lemaire K, Van de Velde S, Van Dijck P, Thevelein JM. Glucose and sucrose act as agonist and mannose as antagonist ligands of the G protein-coupled receptor Gpr1 in the yeast *Saccharomyces cerevisiae*. Mol. Cell. 2004; 16:293–299. [PubMed: 15494315]
72. Amberg GC, Rossow CF, Navedo MF, Santana LF. NFATc3 regulates Kv2.1 expression in arterial smooth muscle. J. Biol. Chem. 2004; 279:47326–47334. [PubMed: 15322114]
73. Nieves-Cintrón M, Amberg GC, Nichols CB, Molkentin JD, Santana LF. Activation of NFATc3 down-regulates the β1 subunit of large conductance, calcium-activated K^+ channels in arterial smooth muscle and contributes to hypertension. J. Biol. Chem. 2007; 282:3231–3240. [PubMed: 17148444]
74. Kim F, Pham M, Maloney E, Rizzo NO, Morton GJ, Wisse BE, Kirk EA, Chait A, Schwartz MW. Vascular inflammation, insulin resistance, and reduced nitric oxide production precede the onset of peripheral insulin resistance. Arterioscler. Thromb. Vasc. Biol. 2008; 28:1982–1988. [PubMed: 18772497]
75. Takeda Y, Nystoriak MA, Nieves-Cintrón M, Santana LF, Navedo MF. Relationship between Ca^{2+} sparklets and sarcoplasmic reticulum Ca^{2+} load and release in rat cerebral arterial smooth muscle. Am. J. Physiol. Heart Circ. Physiol. 2011; 301:H2285–H2294. [PubMed: 21984539]
76. Hall DD, Dai S, Tseng P-Y, Malik Z, Nguyen M, Matt L, Schnizler K, Shephard A, Mohapatra DP, Tsuruta F, Dolmetsch RE, Christel CJ, Lee A, Burette A, Weinberg RJ, Hell JW. Competition between α-actinin and Ca^{2+}-calmodulin controls surface retention of the L-type Ca^{2+} channel $Ca_V1.2$. Neuron. 2013; 78:483–497. [PubMed: 23664615]
77. Dixon RE, Moreno CM, Yuan C, Opitz-Araya X, Binder MD, Navedo MF, Santana LF. Graded Ca^{2+}/calmodulin-dependent coupling of voltage-gated $Ca_V1.2$ channels. eLife. 2015; 4:e05608.
78. Mercado J, Baylie R, Navedo MF, Yuan C, Scott JD, Nelson MT, Brayden JE, Santana LF. Local control of TRPV4 channels by AKAP150-targeted PKC in arterial smooth muscle. J. Gen. Physiol. 2014; 143:559–575. [PubMed: 24778429]
79. Harraz OF, Visser F, Brett SE, Goldman D, Zechariah A, Hashad AM, Menon BK, Watson T, Starreveld Y, Welsh DG. $Ca_V1.2/Ca_V3.x$ channels mediate divergent vasomotor responses in human cerebral arteries. J. Gen. Physiol. 2015; 145:405–418. [PubMed: 25918359]
80. Cheng EP, Yuan C, Navedo MF, Dixon RE, Nieves-Cintrón M, Scott JD, Santana LF. Restoration of normal L-type Ca^{2+} channel function during Timothy syndrome by ablation of an anchoring protein. Circ. Res. 2011; 109:255–261. [PubMed: 21700933]

81. Dixon RE, Yuan C, Cheng EP, Navedo MF, Santana LF. Ca^{2+} signaling amplification by oligomerization of L-type $Ca_V1.2$ channels. Proc. Natl. Acad. Sci. U.S.A. 2012; 109:1749–1754. [PubMed: 22307641]

82. Navedo MF, Cheng EP, Yuan C, Votaw S, Molkentin JD, Scott JD, Santana LF. Increased coupled gating of L-type Ca^{2+} channels during hypertension and Timothy syndrome. Circ. Res. 2010; 106:748–756. [PubMed: 20110531]

83. Hess P, Lansman JB, Tsien RW. Calcium channel selectivity for divalent and monovalent cations. Voltage and concentration dependence of single channel current in ventricular heart cells. J. Gen. Physiol. 1986; 88:293–319. [PubMed: 2428919]

84. Zampini V, Valli P, Zucca G, Masetto S. Single-channel L-type Ca^{2+} currents in chicken embryo semicircular canal type I and type II hair cells. J. Neurophysiol. 2006; 96:602–612. [PubMed: 16687612]

85. Yue DT, Marban E. Permeation in the dihydropyridine-sensitive calcium channel. Multi-ion occupancy but no anomalous mole-fraction effect between Ba^{2+} and Ca^{2+} J. Gen. Physiol. 1990; 95:911–939. [PubMed: 2163433]

86. Nystoriak MA, O'Connor KP, Sonkusare SK, Brayden JE, Nelson MT, Wellman GC. Fundamental increase in pressure-dependent constriction of brain parenchymal arterioles from subarachnoid hemorrhage model rats due to membrane depolarization. Am. J. Physiol. Heart Circ. Physiol. 2011; 300:H803–H812. [PubMed: 21148767]

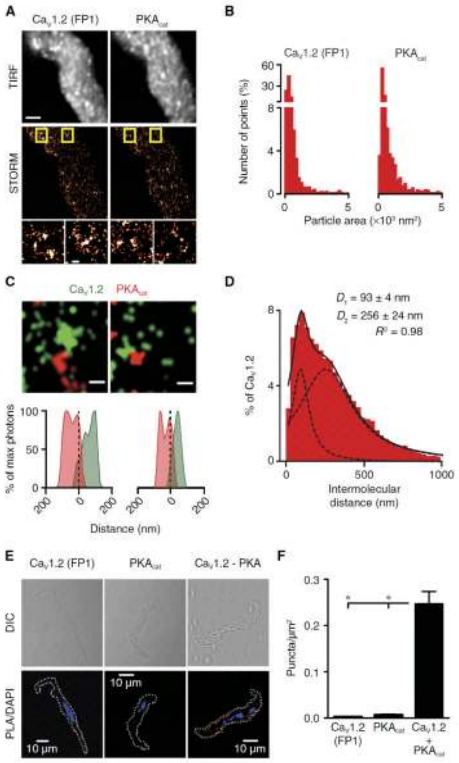

Fig. 1. Spatial organization of $Ca_V1.2$ and PKA in murine arterial myocytes

(**A**) Representative conventional TIRF images (top) and corresponding STORM reconstruction maps (bottom) from a murine arterial myocyte labeled for $Ca_V1.2$ and PKA_{cat} (scale bar, 2 μm). Lower panels are enhanced magnification of areas shown in yellow boxes (scale bar, 100 nm). (**B**) Histograms showing the area of clusters of $Ca_V1.2$ channels and PKA_{cat} in isolated arterial myocytes. (**C**) Expanded merged images (top) and associated *x-y* fluorescence intensity profiles (bottom) of sites of close interaction between $Ca_V1.2$ (green) and PKA_{cat} (red; scale bars, 100 nm). (**D**) Histogram of the lowest intermolecular distance to PKA_{cat} centroids for $Ca_V1.2$ fluorescence particles. Data were fit with a sum of two Gaussian functions with depicted R^2 and centroids (n = 10,306 particles from nine cells). Differential interference contrast (DIC; top) and fluorescence PLA (red)/4′,6-diamidino-2-phenylin-dole (DAPI) (blue) images (**E**) and quantification of PLA fluorescent puncta per square micrometer cell area for isolated arterial myocytes (**F**) labeled for $Ca_V1.2$ (n = 20 cells), PKA_{cat} (n = 18 cells), or $Ca_V1.2$ + PKA_{cat} (n = 19 cells).

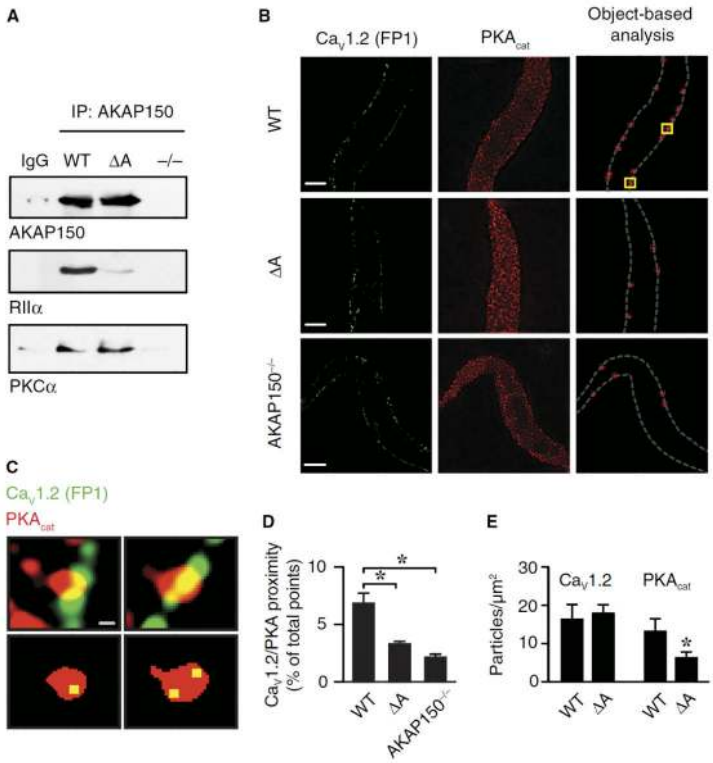

Fig. 2. AKAP150 targets PKA to a subpopulation of $Ca_V1.2$ channels in arterial myocytes

(**A**) Representative immunoprecipitation (IP) of AKAP150 followed by immunoblot detection of AKAP150, PKA RIIα, and PKCα in lysates from wild-type (WT), ΔA, and *AKAP150*$^{-/-}$ mice ($n = 3$ lysates). (**B**) Representative SIM reconstructions of isolated WT, ΔA, and *AKAP150*$^{-/-}$ arterial myocytes labeled with antibodies against $Ca_V1.2$ and PKA_{cat}. Object-based analysis shows location of objects (red crosses) corresponding to $Ca_V1.2$ and PKA_{cat} fluorescence overlap. Scale bars, 5 μm. (**C**) Enlarged SIM (upper) and associated object-based colocalization (lower) images for $Ca_V1.2$ (yellow centroids) and PKA_{cat} (red particles) of regions marked by yellow boxes in image in (B). Scale bar, 200 nm. (**D**) Percentage of total $Ca_V1.2$ channels associated with PKA_{cat} at a distance of <100 nm for WT ($n = 7$ cells), ΔA ($n = 6$ cells), and *AKAP150*$^{-/-}$ ($n = 8$ cells) arterial myocytes (*$P <$ 0.05, Kruskal-Wallis test). (**E**) Summary bar plot showing the density of sarcolemma-associated particles of $Ca_V1.2$ and PKA_{cat} in TIRF/STORM images for arterial myocytes from WT ($n = 6$ cells) and ΔA ($n = 9$ cells) animals (*$P < 0.05$, unpaired t test of WT PKA_{cat} versus ΔA PKA_{cat}).

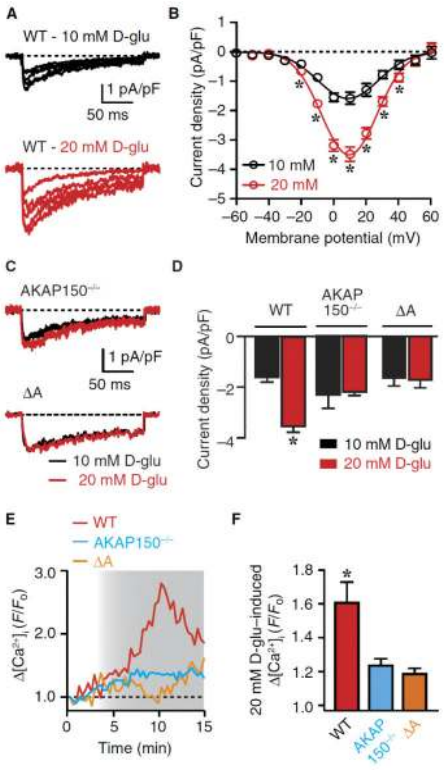

Fig. 3. Enhanced $Ca_V1.2$ channel activity and elevation of global $[Ca^{2+}]_i$ in arterial myocytes in response to 20 mM D-glucose require anchoring of PKA by AKAP150

(**A**) Representative I_{Ba} in WT arterial myocytes evoked by 200-ms depolarization steps from holding potential of −70 mV to voltages ranging from −20 to +40 mV in 10 mM D-glucose (D-glu) and 5 min after application of 20 mM D-glucose. (**B**) I_{Ba}-voltage relationship (−60 to +60 mV) in WT arterial myocytes in the presence of 10 and 20 mM D-glucose ($n = 8$ cells; $^*P < 0.05$, paired t test). (**C**) Representative I_{Ba} from ΔA and *AKAP150*$^{-/-}$ arterial myocytes in response to step depolarizations from −70 to +10 mV before and after application of 20 mM D-glucose. (**D**) Amalgamated I_{Ba} (to +10 mV) before and after application of 20 mM D-glucose in WT, ΔA, and *AKAP150*$^{-/-}$ arterial myocytes ($n = 8$ to 11 cells; $^*P < 0.05$, paired t test). (**E**) Exemplary $[Ca^{2+}]_i$ traces in isolated WT, *AKAP150*$^{-/-}$, and ΔA arterial myocytes in the presence of 10 mM D-glucose and in response to 20 mM D-glucose in shaded time frame. (**F**) Plot of change in Ca^{2+} (F/F_o) to 20 mM D-glucose in isolated WT ($n = 7$ cells), *AKAP150*$^{-/-}$ ($n = 8$ cells), and ΔA ($n = 7$ cells) arterial myocytes [$^*P < 0.05$; one-way analysis of variance (ANOVA) with Tukey post hoc test].

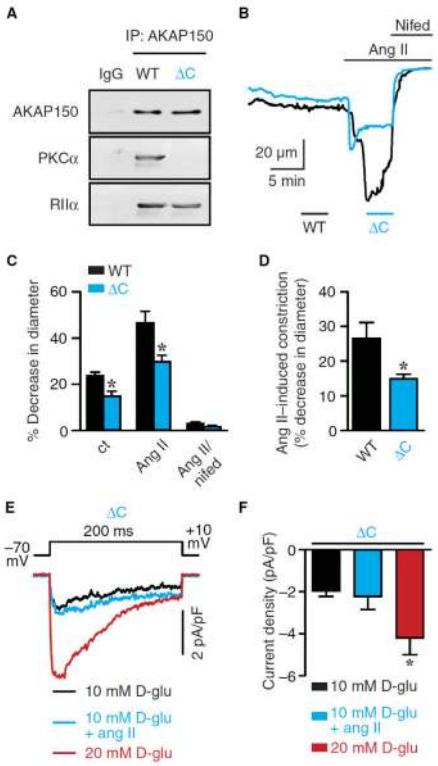

Fig. 4. Anchoring of PKC by AKAP150 is necessary for angiotensin II, but not potentiation of $Ca_V1.2$ channel activity in response to elevated glucose in arterial myocytes

(**A**) Immunoprecipitation of AKAP150 from arterial lysates from WT and ΔC animals followed by immunoblot detection of AKAP150, PKCα, and PKA RIIα ($n = 3$ lysates). (**B**) Representative diameter recordings in pressurized arteries (60 mmHg) before and after application of 100 nM angiotensin II (Ang II) with subsequent application of 1 μM nifedipine (Nifed) from WT ($n = 5$ arteries from three animals) and ΔC ($n = 6$ arteries from four animals) middle cerebral arteries (starting and passive diameters for representative recordings: 118 and 147 μm for WT and 109 and 136 μm for ΔC, respectively). (**C** and **D**) Summary vascular tone data in the absence (ct) and presence of angiotensin II and angiotensin II + nifedipine (C), and angiotensin II–induced constriction (D) in arteries from WT and ΔC mice (*$P < 0.05$, Mann-Whitney U test). (**E**) Representative I_{Ba} from ΔC arterial myocytes in response to step depolarizations to +10 mV from a holding potential of −70 mV before and after application of angiotensin II or 20 mM D-glucose ($n = 8$ cells per condition). (**F**) Summary I_{Ba} data from ΔC arterial myocytes before and after application of angiotensin II or 20 mM D-glucose (*$P < 0.05$, one-way ANOVA with Tukey post hoc test).

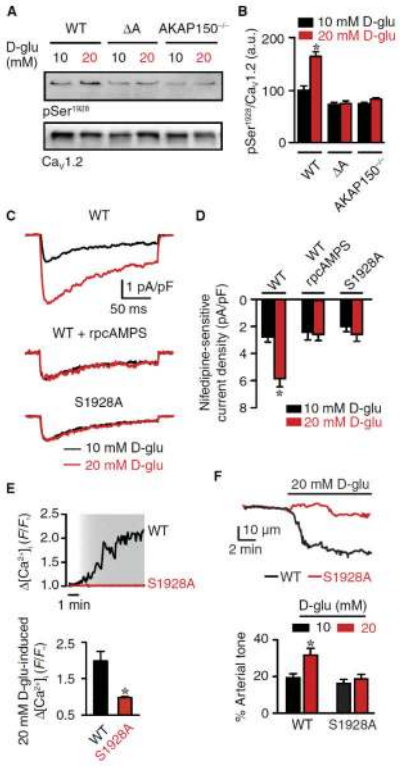

Fig. 5. Phosphorylation of Ser^{1928} by AKAP150-targeted PKA is required for increased Ca$_V$1.2 channel activity, enhanced global [Ca^{2+}]$_i$, and vasoconstriction in response to 20 mM D-glucose in arterial myocytes

(**A**) Representative immunoblot detection of phosphorylated Ser^{1928} (pSer^{1928}) and total Ca$_V$1.2 from WT, ΔA, and *AKAP150*$^{-/-}$ arteries after incubation with D-glucose concentrations, as indicated. (**B**) Quantification by densitometric analysis of pSer^{1928} normalized to total respective Ca$_V$1.2 for WT, ΔA, and *AKAP150*$^{-/-}$ arteries incubated with either 10 or 20 mM D-glucose ($n = 4$ arterial lysates per condition; $^*P < 0.05$, Mann-Whitney *U* test). a.u., arbitrary units. (**C**) Characteristic I_{Ba} recordings from WT, WT + 10 μM rpcAMPS, and S1928A arterial myocytes in response to step depolarizations to +10 mV from a holding potential of −70 mV before (10 mM D-glucose) and after application of 20 mM D-glucose. (**D**) Summary data showing I_{Ba} for WT ($n = 10$ cells), WT + rpcAMPS ($n = 5$ cells), and S1928A ($n = 9$ cells) arterial myocytes in 10 and 20 mM D-glucose ($^*P < 0.05$, paired *t* test). (**E**) Representative fluorescence traces showing global [Ca^{2+}]$_i$ and plot of changes in global [Ca^{2+}]$_i$ in response to 20 mM D-glucose (shaded area) in isolated WT ($n = 9$ cells) and S1928A ($n = 11$ cells) arterial myocytes ($^*P < 0.05$, unpaired *t* test). (**F**) Representative diameter recordings and summary arterial tone (percent decrease in diameter from maximum passive diameter) data from pressurized (60 mmHg) WT and S1928A arteries in response to increasing extracellular D-glucose from 10 to 20 mM ($n = 6$ arteries per condition). Starting and passive diameters for representative recordings: 111 and 132 μm for WT and 126 and 155 μm for S1928A, respectively ($^*P < 0.05$, Wilcoxon matched-pairs signed-rank test).

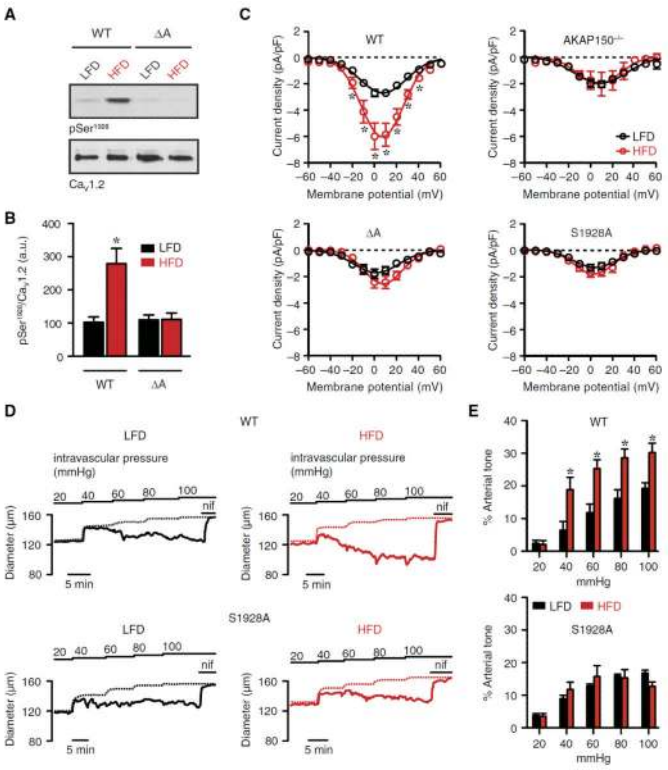

Fig. 6. Increased $Ca_V1.2$ channel activity and enhanced vascular tone during diabetes require AKAP150-PKA phosphorylation of $\alpha1_C$ at Ser^{1928} in vivo

(**A**) Representative immunoblot detection of $pSer^{1928}$ and total $Ca_V1.2$ in arteries isolated from WT and ΔA LFD and HFD animals. (**B**) Densitometric quantification of $pSer^{1928}$/$Ca_V1.2$ ratio in lysates from WT and S1928A LFD and HFD mice ($n = 3$ lysates from three mice per condition) (*$P < 0.05$, Mann-Whitney U test). (**C**) I_{Ba}-voltage relationship (−60 to +60 mV) in arterial myocytes from WT (LFD, $n = 14$ cells from five mice; HFD, $n = 9$ cells from five mice), *AKAP150*$^{-/-}$ (LFD, $n = 5$ cells from two mice; HFD, $n = 5$ cells from two mice), ΔA (LFD, $n = 6$ cells from three mice; HFD, $n = 6$ cells from two mice), and S1928A (LFD, $n = 8$ cells from three mice; HFD, $n = 9$ cells from three mice) mice in LFD and HFD (*$P < 0.05$, unpaired t test). (**D**) Representative diameter records obtained using arteries isolated from WT and S1928A mice in LFD and HFD over a range of intravascular pressures from 20 to 100 mmHg. Arteries were exposed to 1 μM nifedipine at 100 mmHg to assess contribution of $Ca_V1.2$-mediated Ca^{2+} influx to tone generation in each group. (**E**) Bar plots summarizing arterial tone, expressed as a percent decrease in diameter from maximum passive diameter at a given pressure for arteries in WT and S1928A mice in LFD and HFD ($n = 7$ to 8 arteries from three animals per group; *$P < 0.05$, Mann-Whitney U test).

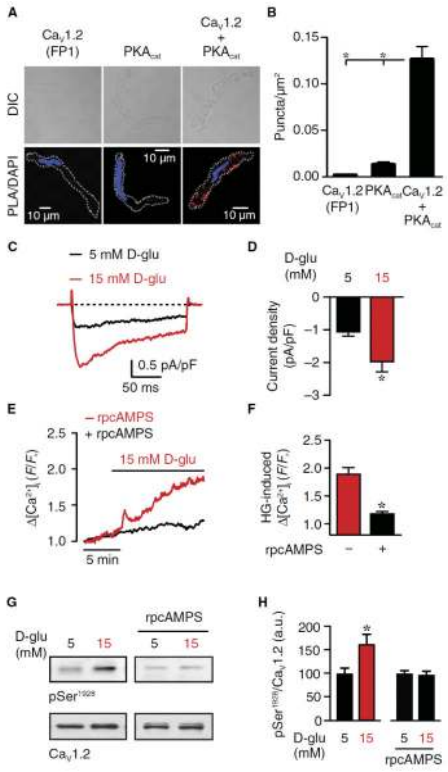

Fig. 7. A subpopulation of $Ca_V1.2$ associates with PKA to stimulate $Ca_V1.2$ channel activity, global Ca^{2+}, and Ser^{1928} phosphorylation in response to elevated glucose in native human arterial myocytes

(**A**) Differential interference contrast (top) and fluorescence PLA (red)/DAPI (blue) images of freshly dissociated human arterial myocytes labeled for $Ca_V1.2$ or PKA_{cat} or $Ca_V1.2$ + PKA_{cat} from nondiabetic patients. (**B**) Quantification of PLA fluorescent puncta per square micrometer cell area for human arterial myocytes labeled for $Ca_V1.2$ ($n = 14$ cells), PKA_{cat} ($n = 15$ cells), and $Ca_V1.2$ + PKA_{cat} ($n = 16$ cells) (*$P < 0.05$, one-way ANOVA with Tukey post hoc test). I_{Ba} records (from −70 to +10 mV) (**C**) and amalgamated current density data (**D**) obtained from freshly dissociated human arterial myocytes from nondiabetic subjects exposed to 5 and 15 mM D-glucose ($n = 7$ cells from three patients) (*$P < 0.05$, paired t test). (**E** and **F**) $[Ca^{2+}]_i$ records and summary data of the response (F/F_0) to increasing bath D-glucose from 5 to 15 mM in freshly dissociated arterial myocytes from nondiabetic subjects in the absence ($n = 11$ cells from four patients) or presence ($n = 9$ cells from two patients) of 10 μM rpcAMPS (*$P < 0.05$, unpaired t test). (**G**) Immunoblot detection of $pSer^{1928}$ and total $Ca_V1.2$ in human arteries incubated (10 min) with 5 or 15 mM D-glucose in the absence or presence of rpcAMPS. (**H**) Normalized densitometric quantification of $pSer^{1928}$ relative to total $Ca_V1.2$ ($n = 4$ lysates from four patients for each) (*$P < 0.05$, Mann-Whitney U test).

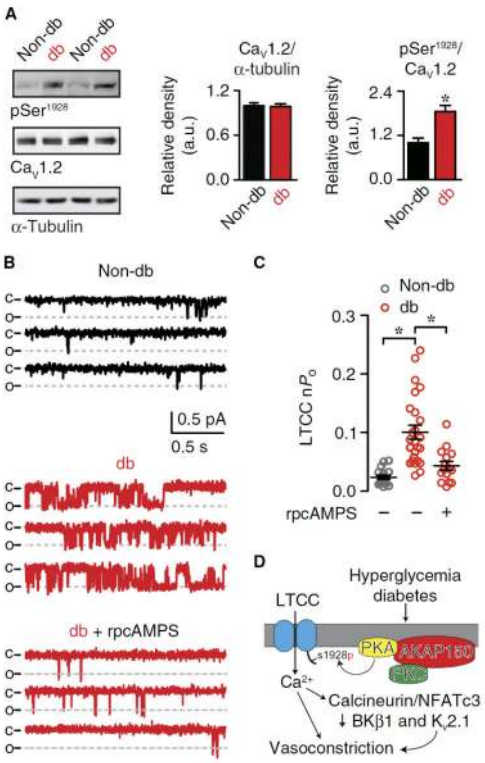

Fig. 8. Arterial myocytes from diabetic patients exhibit enhanced Ser^{1928} phosphorylation and PKA-dependent augmentation of Ca$_V$1.2 channel activity

(**A**) Representative immunoblot detection of pSer^{1928}, total Ca$_V$1.2, and α-tubulin and densitometric summary data for total Ca$_V$1.2 (relative to α-tubulin) and pSer^{1928} (relative to total Ca$_V$1.2) in arterial lysates isolated from nondiabetic ($n = 4$) and diabetic patients ($n = 4$) (*$P < 0.05$, Mann-Whitney U test). (**B**) Representative elementary Ca$_V$1.2 channel records obtained during a 2-s step depolarization from −80 to −30 mV in freshly dissociated human arterial myocytes from non-diabetic (Non-db) and diabetic (db; ±10 μM rpcAMPS) patients. Channel openings (o) are represented by downward deflections from baseline (c). (**C**) Plot shows Ca$_V$1.2 channel nP_o for cells from nondiabetic patients ($n = 27$ cells from six patients) and diabetic patients in the absence ($n = 24$ from four patients) or presence ($n = 14$ cells from three patients) of rpcAMPS (*$P < 0.05$, Kruskal-Wallis test). LTCC, L-type Ca^{2+} channel. (**D**) Proposed model of Ca$_V$1.2 channel stimulation upon increases in extracellular glucose and in diabetes.